Roles of the ocean mesoscale in the horizontal supply of mass, heat, carbon and nutrients to the Northern Hemisphere subtropical gyres

Ayako Yamamoto[1] *, Jaime B. Palter[1,2], Carolina O. Dufour[1,3], Stephen M. Griffies[4], Daniele Bianchi[5], Mariona Claret[6], John P. Dunne[4], Ivy Frenger[7], Eric D. Galbraith[8,9]

Ayako Yamamoto, ayako.yamamoto@jamstec.go.jp

[1]Department of Atmospheric and Oceanic Sciences, McGill University, Montreal, Quebec, Canada.

[2]Graduate School of Oceanography, University of Rhode Island, Narragansett, Rhode Island, USA.

[3]Atmospheric and Oceanic Sciences Program, Princeton University, Princeton, New Jersey, USA.

[4]NOAA/Geophysical Fluid Dynamics Laboratory, Princeton, New Jersey, USA.

This article has been accepted for publication and undergone full peer review but has not been through the copyediting, typesetting, pagination and proofreading process, which may lead to differences between this version and the Version of Record. Please cite this article as doi: 10.1029/2018JC013969

Abstract.

Horizontal transport at the boundaries of the subtropical gyres plays a crucial role in providing the nutrients that fuel gyre primary productivity, the heat that helps restratify the surface mixed layer, and the dissolved inorganic carbon (DIC) that influences air-sea carbon exchange. Mesoscale eddies may

[5]Department of Atmospheric and Oceanic Sciences, University of California, Los Angeles, Los Angeles, California, USA.

[6]Joint Institute for the Study of the Atmosphere and Ocean, University of Washington, Seattle, Washington, USA.

[7]GEOMAR Helmholtz Centre for Ocean Research, Kiel, Germany.

[8]Institut de Ciència i Tecnologia Ambientals (ICTA) and Department of Mathematics, Universitat Autonoma de Barcelona, Barcelona, Spain.

[9]Institució Catalana de Recerca i Estudis Avançats (ICREA), Barcelona, Spain.

[*]Current affiliation: Japan Agency for Marine-Earth Science and Technology, Yokohama, Japan

be an important component of these horizontal transports; however, previous studies have not quantified the horizontal tracer transport due to eddies across the subtropical gyre boundaries. Here we assess the physical mechanisms that control the horizontal transport of mass, heat, nutrients and carbon across the North Pacific and North Atlantic subtropical gyre boundaries using the eddy-rich ocean component of a climate model (GFDL's CM2.6) coupled to a simple biogeochemical model (mini-BLING). Our results suggest that horizontal transport across the gyre boundaries supplies a substantial amount of mass and tracers to the ventilated layer of both Northern Hemisphere subtropical gyres, with the Kuroshio and Gulf Stream acting as main exchange gateways. Mass, heat, and DIC supply is principally driven by the time-mean circulation, whereas nutrient transport differs markedly from the other tracers, as nutrients are mainly supplied to both subtropical gyres by down-gradient eddy mixing across gyre boundaries. A budget analysis further reveals that the horizontal nutrient transport, combining the roles of both mean and eddy components, is responsible for more than three quarters of the total nutrient supply into the subtropical gyres, surpassing a recent estimate based on a coarse resolution model and thus further highlighting the importance of horizontal nutrient transport.

1. Introduction

The dynamics of the primarily wind-driven upper kilometre of the ocean's subtropical gyres play a critical role in regulating the climate, ocean carbon dioxide (CO_2) uptake, and the subtropical ecosystem [*Huang and Qiu*, 1994; *McClain et al.*, 2004]. More than a third of the Earth's total meridional heat transport at the latitudes of the subtropical gyres is carried by the ocean, and the convergence of this oceanic heat transport at the subtropical gyre latitudes implies vigorous heat loss to the atmosphere [*Trenberth and Caron*, 2001]. Subtropical gyres in the Northern Hemisphere are among the largest carbon uptake regions for the contemporary atmospheric CO_2 on an annual basis, due to the low partial pressures of CO_2 at their surface [*Takahashi et al.*, 2009]. Moreover, subtropical gyres are home to the ocean's largest biome owing to their vast surface area, covering roughly 40% of the global ocean [*McClain et al.*, 2004; *Letscher et al.*, 2016]. Thus, understanding what processes supply heat, carbon, and nutrients to the subtropical gyres is critical to characterize ocean climate, biogeochemistry, and ecology.

In contrast to the neighbouring subpolar gyres and the tropics, where large-scale Ekman suction upwells cold, nutrient-rich water, the subtropical gyres are regions of large-scale downwelling that deepens the thermocline and nutricline [*Williams and Follows*, 1998; *Wilson and Coles*, 2005; *Omand and Mahadevan*, 2015]. The contrasting dynamics of the subtropical gyres and their surroundings leads to strong property gradients at the gyre boundaries. Thus, it is natural to hypothesize that cross-boundary exchange could have profound implications for gyre tracer budgets [*Bower et al.*, 1985; *Williams and Follows*, 1998; *Ayers and Lozier*, 2010; *Palter et al.*, 2013]. This cross-boundary exchange, however,

is extremely challenging to measure directly, and most global ocean models cannot resolve the mesoscale eddying motions that are ubiquitous at these boundaries, being forced to parameterize their effects instead. Here, we explore the role of cross-boundary exchange on heat, carbon and nutrient budgets, making use of a climate model that resolves a rich spectrum of ocean mesoscale eddies in the subtropics [*Delworth et al.*, 2012; *Griffies et al.*, 2015] and is coupled to a simplified biogeochemical model [*Galbraith et al.*, 2015].

For instance, since cross-boundary heat exchange can influence the subtropical mixed layer temperature, such exchange may impact the reemergence of climate signals, whereby wintertime thermal anomalies sequestered in the deep mixed layer are re-entrained into the mixed layer in the following winter [*Alexander and Deser*, 1995]. Such reemergence of thermal anomalies is thought to possibly cause persistence of climate signals, such as the North Atlantic Oscillation, on interannual and longer time scales [*Kwon et al.*, 2010; *Cassou et al.*, 2007]. In addition to the potential role of heat supply to the subtropics on climate variability, cross-boundary heat exchange also influences the solubility of CO_2 in the surface waters. Moreover, anomalies of dissolved inorganic carbon (DIC) crossing the subtropical gyre boundaries can further influence the subtropical uptake of atmospheric CO_2 within the ocean [*Ayers and Lozier*, 2012].

The dynamical supply of nutrients into the subtropical euphotic zone was once thought to be dominated by vertical processes such as mixing and advection from intermediate depths. This paradigm, however, gave rise to a long standing puzzle, as new production outpaced the known vertical supply of nutrients to the subtropical gyre euphotic zone [e.g., *McGillicuddy Jr et al.*, 1998; *Oschlies and Garçon*, 1998]. An increasing number of recent studies have replaced this paradigm with one that includes horizontal processes in supply-

ing nutrients to the subtropical gyre from the neighbouring nutrient-rich subpolar gyres and tropics [*Williams and Follows*, 1998, 2003; *Oschlies*, 2002; *Ayers and Lozier*, 2010; *Palter et al.*, 2013]. Recently, *Letscher et al.* [2016] used an observationally-constrained, coarse-resolution model to propose that roughly half of the dissolved inorganic phosphate (PO_4) required to close the nutrient budgets in the subtropical gyres is supplied by horizontal transport. Understanding horizontal transport of PO_4 into the subtropical gyres is further motivated by recent studies which revealed that subtropical phytoplankton have elevated carbon to phosphorus ratios, implying a greater organic carbon transport to the deep ocean for every mole of PO_4 that enters the gyre than if it were consumed elsewhere [*Teng et al.*, 2014; *Galbraith and Martiny*, 2015]. This high carbon ratio in subtropical export productivity also has implications for the oceanic storage and air-sea partitioning of CO_2. Despite advances in understanding the role of horizontal circulation in subtropical nutrient supply, important questions remain unanswered: Where is the horizontal exchange strongest? And what is the role of mesoscale eddies?

One reason the answers to these questions have remained elusive is that they require observations or models that resolve swift boundary currents and the mesoscale eddies associated with them. These oceanic jets, which mark the western edges of the subtropical gyres, are known to be the regions which serve as both "blender" and "barrier" for cross-frontal tracer exchanges [*Bower et al.*, 1985]. On the one hand, the jets act as "blender" for tracers, in part due to strong down-front westerly winds that drive Ekman transport across the currents [e.g., *Williams and Follows*, 1998; *Ayers and Lozier*, 2010; *Palter et al.*, 2011, 2013]. Furthermore, these highly baroclinic western boundary currents are regions of enhanced mesoscale eddy activity due to the heightened available potential energy

[*Williams and Follows*, 2003; *Griffies et al.*, 2015]. These mesoscale motions, collectively referred to as eddies, are ubiquitous features in the ocean and persist over time scales of weeks to months and horizontal scales from tens to hundreds of kilometres [*Bishop et al.*, 2013]. Eddies, including rings shed from frontal systems, can induce significant cross-frontal exchange [*Samelson*, 1992; *Lee and Williams*, 2000; *Qiu et al.*, 2007]. Observational studies have estimated that such eddy structures transport a substantial amount of heat and salt [*Zhang et al.*, 2014; *Dong et al.*, 2014; *Sasaki and Minobe*, 2015]. On the other hand, the swift currents associated with these oceanic jets are thought to act as "barriers" for tracer exchange by suppressing eddy-driven mixing at the shallower depths, where the speed of the jet is much faster than the propagation speed of its meanders [*Bower et al.*, 1985; *Bower*, 1991; *Samelson*, 1992; *Smith and Marshall*, 2009; *Ferrari and Nikurashin*, 2010; *Dufour et al.*, 2015]. The role of eddies in the subtropical gyres, however, has not been fully resolved.

Previous studies addressing similar questions for the horizontal supply of nutrients across the western boundary currents were conducted with the use of either an idealized model [*Lee and Williams*, 2000], an order-of-magnitude assessment based on observations [*Palter et al.*, 2013], or an observationally-constrained coarse resolution model [*Letscher et al.*, 2016]. Thus, the role of eddies for the subtropical gyre's nutrient budget has not been explicitly quantified, and the role of eddies in mass, heat and DIC transport has been missing. Furthermore, while the rings shed from the Kuroshio are thought to play a significant role in the potential vorticity budget in the North Pacific subtropical gyre region [*Qiu and Chen*, 2006; *Qiu et al.*, 2007], rings shed from the Gulf Stream may play only a minor role in the subtropical tracer budgets [*Bower et al.*, 1985]. Given these con-

trasting properties of western boundary currents and the conflicting reports on the impact of mesoscale rings in tracer budgets over the two Northern Hemisphere subtropical gyre basins, it is difficult to anticipate the role of mesoscale motion in the horizontal transport of mass and tracers into subtropical gyres without a model that resolves these motions.

The purpose of this work is to quantify the horizontal transport of heat, carbon, and nutrients into the North Pacific and North Atlantic subtropical gyres. Our ultimate goals are to assess the physical mechanisms that control the transport of these tracers into the interior of the subtropical gyres all along their boundaries; evaluate their importance in gyre heat, DIC, and nutrient budgets; and understand the spatial variability of these transports, as well as any contrast that may emerge between the North Atlantic and the North Pacific subtropical gyres. In order to achieve these goals, we use a preindustrial control simulation from an eddy-rich ocean-atmosphere climate model coupled to a simple marine biogeochemical model (CM2.6-miniBLING). We quantify the annual transport across the boundaries of the subtropical gyres and further decompose it into mean and eddy components. CM2.6-miniBLING provides an adequate tool for our purposes, with its horizontal resolution of 0.1° allowing us to sufficiently resolve the mesoscale eddies of interest.

The rest of the paper is organized as follows. In Section 2, we describe the model used (Section 2.1), our definition of the horizontal (Section 2.2.1) and vertical extent of the subtropical gyres (Section 2.2.2), and the decomposition of the tracer transport across the gyre boundaries into mean and eddy components (Section 2.3). In Section 3, we discuss the hot spots of the horizontal mass transport (Section 3.1), relative roles of advection and down-gradient mixing in the horizontal tracer supply to the subtropical

gyres (Section 3.2), and the contribution of horizontal transport to the tracer budgets in the subtropical gyres (Section 3.3). A discussion and conclusion are provided in Section 4.

2. Methods

2.1. CM2.6-miniBLING

Our primary tool is an eddy-rich coupled climate model, Geophysical Fluid Dynamics Laboratory (GFDL) Climate Model version 2.6 (CM2.6) [*Delworth et al.*, 2012; *Griffies et al.*, 2015], coupled to a simplified version of the Biogeochemistry with Light Iron Nutrients and Gas (miniBLING) model [*Galbraith et al.*, 2015]. The atmospheric, sea ice and land components of CM2.6 each have a horizontal resolution of 0.5°, whereas the oceanic component has 0.1° resolution. The horizontal resolution in the model is fine enough to represent a rich spectrum of mesoscale eddies in the ocean, and the resulting modelled eddy kinetic energy matches closely that calculated from altimetric observations of the sea surface in the subtropics, as shown in *Delworth et al.* [2012] and *Griffies et al.* [2015]. Therefore, the model faithfully represents the strength of the eddy field in the region and can be regarded as "eddy-resolving" at these locations [*Hallberg*, 2013]. The ocean component of the climate model is based on the Modular Ocean Model, version 5 (MOM5) [*Griffies*, 2012], configured using the Boussinesq approximation with 50 vertical levels and the z* vertical coordinate. The vertical cell thickness increases from roughly 10 m in the upper ocean to 210 m in the deep ocean. There is neither lateral tracer diffusion nor a mesoscale eddy parameterization in this model. However, submesoscale mixed layer eddy transport is parameterized according to *Fox-Kemper et al.* [2011]. Vertical mixing processes are parameterized in the model using the K-profile parameterization scheme

[*Large et al.*, 1994], an internal gravity wave breaking scheme [*Simmons et al.*, 2004], as well as the coastal tide mixing scheme [*Lee et al.*, 2006].

MiniBLING is a simplified version of the prognostic biogeochemical model, BLING [*Galbraith et al.*, 2010], developed in order to reduce computational cost for use in eddy-resolving models, while still simulating essential aspects of bulk ecosystem dynamics [*Galbraith et al.*, 2015]. Its three prognostic tracers are dissolved inorganic carbon (DIC), dissolved oxygen (O_2), and a macronutrient that is initialized from a nutrient climatology as the average of phosphate (PO_4) and nitrate (NO_3), weighted according to their Redfield ratios ($PO_4/2 + NO_3/32$). Therefore, the macronutrient concentrations have values similar to oceanic PO_4 concentrations. Also, because there is no representation of nitrogen fixation or denitrification, this nutrient tracer is more indicative of PO_4 cycling, and hereafter we refer to this macronutrient as "PO_4". By acting as the limiting macronutrient in the subtropics, however, the nutrient tracer may behave more like NO_3. The reduction of the number of prognostic tracers was achieved by removing dissolved organic matter, the prognostic iron tracer, and the prognostic alkalinity tracer from the original BLING biogeochemical model. To deal with the absence of a dissolved organic phosphorus pool, the model has a fast-recycling term to return organic phosphorus to phosphate. Alkalinity is diagnosed from a climatological alkalinity-salinity relationship, and the iron cycle has been replaced by prescribing a monthly iron climatology generated by a 1° version of the climate model ESM2M using BLING [*Galbraith et al.*, 2015]. Despite some biases, including the seasonal cycle of biomass and export production in comparison to the more comprehensive model TOPAZ, miniBLING was shown to successfully simulate large-scale biogeochemical annual cycling at the global scale in EMS2M [*Galbraith et al.*, 2015].

The CM2.6-miniBLING preindustrial control simulation is run with atmospheric CO_2 fixed at the preindustrial concentration of 286 ppm. The simulation is run for 200 years starting from rest, with the miniBLING component being included from year 48. Temperature, salinity, PO_4 and O_2 fields are initialized with data from the World Ocean Atlas 2009 (WOA) [*Locarnini et al.*, 2010; *Garcia et al.*, 2010a, b], and DIC fields from the Global Ocean Data Analysis Project (GLODAP), which were adjusted to preindustrial values [*Key et al.*, 2004]. In the following analysis, we utilize the last 10 years of the simulation, corresponding to years 191 to 200. The analysis was limited to ten years due to data storage constraints; however, we assume that the averaging period is long enough to eliminate analysis bias due to most interannual variability, though the averaging period is not long enough to eliminate analysis bias due to decadal fluctuations.

A comparison of the modelled fields and observations is shown in Figure 1. The overall observed global pattern is captured by the model, particularly over the regions of interest indicated by black contours on the panels on the right column. However, some deviations are apparent. In general, the model has a cold bias, while it overestimates the DIC field. The cooler simulated surface temperature compared to the present-day observations is an expected outcome of the model spin-up with the preindustrial level of CO_2. The discrepancy in DIC likely results from the cooler temperature and higher CO_2 solubility. A band-like negative temperature and sea surface height (SSH) anomaly in the North Atlantic suggests a southward shift of the North Atlantic Current in the model relative to the observations, as the Gulf Stream becomes unstable closer to the coast in the simulations than in the observations [see *Griffies et al.*, 2015, and references therein]. In addition, the stationary meander off of Japan is found slightly more southwestward

in the model relative to observations. However, as discussed later in Section 2.2.1, our choice of gyre boundaries uses a dynamical definition based on model fields, so that such misalignment of observed and simulated currents should not influence our interpretation of the processes giving rise to cross-boundary transport.

Furthermore, since our main focus is in the roles played by mesoscale eddies, we also evaluated the skill of the model at simulating the mesoscale variability. To do so, we compared the modelled and observed mean dynamical sea level (DSL) standard deviation along the mean horizontal subtropical gyre boundary defined using a largest closing mean simulated and observed SSH contour as *Palter et al.* [2013] (not shown). The general structure and magnitude of the DSL variance closely agreed in the simulation and satellite observations. The only exception is in the Gulf Stream region, where the simulated mean DSL standard deviation is smaller by approximately 78% on average, and the simulated longitudinal extent of elevated DSL standard deviation is narrower by about 10 degrees in longitude compared to the observations (not shown). These biases likely reflect that the Gulf Stream goes unstable too close to the coast, as discussed above.

Some other potential causes of errors for our cross-gyre boundary study include more pronounced gradients of the modelled nutrients and DIC at the northern subtropical gyre boundary in the North Pacific. This deviation from the observations could induce larger down-gradient eddy-induced tracer mixing in our result compared to the observations. The model, however, adequately captures the magnitude of the cross-gyre contrasts and the spatial scales that separate them. For a detailed comparison of miniBLING to observations and more complex biogeochemical models, readers are referred to *Galbraith et al.* [2015].

2.2. Definition of the Subtropical Gyres

The subtropical gyres are pools of nutrient-depleted warm water, circulating anticyclonically, driven primarily by winds [*Stommel*, 1958] but also by buoyancy forcing in the western boundary current [*Spall*, 1992]. Although the gyres have been the subject of study for decades, there is no standard definition for the subtropical gyre boundaries. For example, previous studies have investigated subtropical gyre properties inferred from hydrographic or satellite observations with a range of definitions, typically based on surface properties, such as chlorophyll content and wind stress curl [*Nicholson et al.*, 2008; *Lozier et al.*, 2011; *Kwon et al.*, 2016; *Oschlies*, 2002; *McClain et al.*, 2004; *Irwin and Oliver*, 2009; *Letscher et al.*, 2016]. Here, we define the subtropical gyre boundaries combining the fundamental ideas that the western edges of the subtropical gyres are the swift western boundary currents, and that the surface of the subtropical gyre contains a pool of warm, well-oxygenated, low-nutrient water, whose vertical limit is marked by the base of the ventilated pycnocline. Thus, the subtropical gyre boundary definition in this study combines both the property-based and dynamical definitions of the subtropical gyres.

2.2.1. Horizontal Extent

In the current study we define the subtropical gyre's horizontal extent using the monthly climatology of the two-dimensional barotropic mass quasi-stream function (Ψ) integrated over the upper 1,000 m. We chose 1,000 m for the base of the quasi-stream function, as our interest lies in the upper ocean. Because the Gulf Stream and Kuroshio extend over a depth of approximately 1,000 m, this definition aligns better with the jets than integrating to the ocean bottom. Note that the true mass stream function is defined only for divergence-free flows, and since the 1,000 m horizontal transport is not required to be divergence-free, we call the integral of this transport the mass quasi-stream function.

Despite choosing a quasi-streamfunction as the subtropical gyre's horizontal boundary, there can still be a time-mean net mass flux across this boundary because a) there is no mandate for non-divergence to the bottom of the layer, and b) as the flow on every level does not match the 1,000-m quasi-streamline exactly, non-divergence at a depth above 1,000 m is not guaranteed. The gyre boundary is insensitive to the depth of integration above 1,000 m. For instance, integrating over the top 500 m instead of 1,000 m does not significantly change the overall gyre's areal extent (not shown).

For each basin, we picked one value of the 10-year monthly mean mass quasi-stream function which encloses the largest areal extent for every month. In this manner, $\Psi = 20$ Sv ($1\ \text{Sv} = 10^9\ \text{kg s}^{-1}$; note that here we use a mass Sverdrup) and $\Psi = 25$ Sv were chosen for the North Pacific and the North Atlantic, respectively (Figure 2). This approach is similar to that used by *Palter et al.* [2013], who defined the subtropical gyre using the largest closed sea surface height contour. This definition of subtropical gyres is dynamical and has the advantage that the boundary is precisely aligned with the monthly-mean meandering jet on the western edges of the subtropical gyre. The qualitative results and interpretation of the mass and tracer transport across these boundaries are not sensitive to which stream function is chosen for the boundary, so long as it is within the swift jet. In contrast, if the chosen boundary did not align with the jet, then any jet meanders across the boundary would appear as local hot-spots of cross-boundary exchange (not shown).

Significant month-to-month variability in the areal extent of the gyres for both basins is evident in Figure 2, ranging from 2.7×10^6 to 6.9×10^6 km^2 in the North Atlantic and 1.2×10^7 to 2.1×10^7 km^2 in the North Pacific. The seasonal meridional shift in the southern

gyre boundaries corresponds to that of the surface wind stress curl (not shown), while the northern gyre boundaries are closely tied to the Gulf Stream and Kuroshio dynamics.

2.2.2. Vertical Extent

We set the vertical limit of our study region to coincide with an isopycnal level just denser (0.1 kg m^{-3}) than the densest isopycnal level that outcrops in March within the subtropical gyre, when mixed layers are deepest. We refer to the layer above this isopycnal as the ventilated pycnocline, following *Luyten et al.* [1983]. By choosing an isopycnal that is just denser than the outcropping isopycnal, we ensure that the horizontal transport of mass and tracers that we wish to quantify are across the horizontal gyre boundary set by the streamline defined in Section 2.2.1, rather than across an isopycnal that outcrops inside that boundary (a summary schematic at the end of the paper, Figure 9, shows the isopycnal and gyre boundary). Additionally, under surface buoyancy loss, vertical fluxes can extend into the stratified interior [*Large et al.*, 1994], so choosing an isopycnal slightly denser than the outcropping density ensures that we capture these fluxes and that we consider all isopycnal layers that are directly ventilted, even if only weakly.

The oxygen cross sections in Figure 3 show that the well-oxygenated layers are found above σ_θ = 25.8 kg m^{-3} (which corresponds to a seawater potential density of 1,025.8 kg m^{-3}) in the North Pacific, and σ_θ = 26.6 kg m^{-3} in the North Atlantic. Thus, we set the base of the vertical layer at these isopycnals, which divide the warm, nutrient- and DIC-depleted, and oxygen-rich upper layer from the cool, nutrient- and DIC-rich, and oxygen-poor lower layer (Figure 3). By definition, this is the deepest layer that the atmosphere can influence directly in the subtropical gyre, and in our analyses we integrate the subtropical gyre properties and the cross-boundary transports from the surface to

these isopycnal levels. The annual-mean depth of the ventilated pycnocline for each basin is shown in Figure 4a and b, illustrating that the deepest layers are found just south of the Gulf Stream and the Kuroshio. Like our horizontal gyre boundaries, the depth of the ventilated pycnocline varies monthly according to a 10-year average seasonal cycle. In both gyres, the maximum area-weighted mean depth is found in late winter (Figure 4c).

This definition of the ventilated pycnocline in both subtropical gyres also encapsulates the subtropical mode water (STMW). STMW is a layer of weakly stratified water and it exists by virtue of wintertime convection at the poleward edge of the subtropical gyres [*Worthington*, 1959; *Hanawa and Talley*, 2001]. At the time of formation, nutrients are consumed at the northern flank of the subtropical gyres in both basins, and this nutrient-depleted water mass is advected southward while being gradually eroded by mixing [*Palter et al.*, 2005; *Oka et al.*, 2015]. STMW in each basin is known to have a characteristic temperature, which is roughly 16 - 19.5°C in the North Pacific [*Masuzawa*, 1969; *Oka et al.*, 2015] and 18°C in the North Atlantic [*Worthington*, 1959]. In the model, these temperatures are found between the isopycnal levels σ_θ = 24.4 - 25.6 kg m^{-3} in the North Pacific, and between σ_θ = 26.2 - 26.4 kg m^{-3} in the North Atlantic (Figure 3), thereby roughly corresponding to our ventilated pycnocline. Thus, the mode waters in the model show similar hydrographic properties as in observations.

2.3. Decomposition of the horizontal transport into mean and eddy components

The horizontal transport of seawater mass and tracer mass through a vertical grid cell face of the horizontal gyre boundaries defined in Section 2.2.1 is written

$$\Phi = \rho_0 dl \hat{\mathbf{n}} \cdot \mathbf{U} C. \tag{1}$$

In this equation, ρ_0 is the constant reference density for the Boussinesq approximation (ρ_0 = 1,035 kg m^{-3}), C is the tracer concentration (set to unity for seawater mass transport), and

$$\mathbf{U} = \mathbf{u}dz \tag{2}$$

is the horizontal velocity field, $\mathbf{u}$, weighted by the grid cell thickness, dz. The normal vector $\hat{\mathbf{n}}$ is perpendicular to the vertical area of the cell face, $dzdl$. The horizontal distance dl is either dx or dy according to the orientation of the gyre boundary. For the subtropical gyres, we choose the normal vector $\hat{\mathbf{n}}$ to point inward, so that a positive transport means mass is added to the gyre interior.

Following *Griffies et al.* [2015] and *Dufour et al.* [2015], we decompose the total horizontal transport averaged over 10 years into two terms:

$$\Phi_{total} = \Phi_{mean} + \Phi_{eddy}. \tag{3}$$

The transport

$$\Phi_{total} = \overline{\Phi} = \rho_0 dl \hat{\mathbf{n}} \cdot \overline{\mathbf{U}C} \tag{4}$$

is the total horizontal transport of seawater mass and tracer mass averaged over 10 years crossing the gyre boundaries. The horizontal gyre boundaries are set according to the monthly climatological quasi-barotropic mass streamfunction (Section 2.2.1), which in turn determines the geometric factors, $dl\hat{\mathbf{n}}$. We accumulate the horizontal tracer transport, $\mathbf{U}C$, every model time step, thus ensuring a proper accounting of temporal correlations. The contribution, Φ_{mean}, measures transport from the time-mean mass transport acting on the time-mean tracer concentration,

$$\Phi_{mean} = \rho_0 dl \hat{\mathbf{n}} \cdot \overline{\mathbf{U}}\,\overline{C} \tag{5}$$

We diagnose the time-mean tracer concentration and time-mean horizontal mass transport directly from the model output for each month, so that the time-mean component captures the 10-year averaged, climatological transport, that accounts for the seasonal cycle. Finally, the eddy component is the residual,

$$\Phi_{eddy} = \Phi_{total} - \Phi_{mean} = \rho_0 dl \hat{\mathbf{n}} \cdot (\overline{\mathbf{U}C} - \overline{\mathbf{U}}\,\overline{C}). \tag{6}$$

This eddy term arises from correlations between fluctuations in tracer concentration and mass transport relative to the climatological monthly-mean transport.

Each of these terms is vertically integrated over the ventilated pycnoclines defined in Section 2.2.2, after binning the total and the mean components onto isopycnal layers from the model's native z* coordinate, following a similar procedure as described in Appendix B of *Dufour et al.* [2015]. The total transport is binned onto each month's mean σ_θ, while the mean component is binned onto the 10-year climatological monthly-mean σ_θ. The correlation of the velocity anomalies with the temporally-varying isopycnal layer thickness gives rise to the eddy mass transport. Our results will reveal that the largest eddy mass and tracer fluxes are found in the jet region, as expected from previous studies [*Griffies et al.*, 2015; *Fratantoni*, 2001] to be a region of high eddy kinetic energy. Thus, we expect that the eddy fluxes are dominated by oceanic mesoscale fluctuations (e.g. waves, rings, vortices, and transient jet meanders). Note that along with the the variability shorter than a month, this definition of the eddy term also contains fluctuations acting on interannual and longer time scales. Since mesoscale variability in fact covers a large span of frequencies, as represented by rings shed from the Kuroshio and Gulf Stream persisting for many months to years as well as the interannual variability in the mesoscale itself [*Qiu*

et al., 2007], it is adequate to include these longer-frequency fluctuations of the mesoscale features in the eddy term.

Baroclinic eddies are one category of motion that gives rise to such mesoscale fluctuations, and there are two key processes associated with these eddies. First, baroclinic eddies act to convert available potential energy (input by wind and buoyancy forcing) to kinetic energy [*Gent et al.*, 1995]. Potential energy reduction flattens isopycnals, and thus reduces thermal wind shear. This adiabatic mesoscale eddy transport opposes the wind-driven time-mean flow. As suggested by *Gent et al.* [1995], this process is commonly parameterized by an eddy-induced advective velocity added to the tracer equation. Therefore, eddies transport mass and tracer by this isopycnal slumping effect, and this tracer transport need not be down-gradient. In addition to slumping isopycnals, mesoscale eddies stir tracers along isopycnals, thus enhancing the fine scale tracer features (i.e., tracer gradients are intensified). In turn, the enhanced fine scale tracer features allow tracers to be efficiently mixed by molecular diffusion. This aspect of mesoscale eddy transport is commonly parameterized by down-gradient isopycnal tracer diffusion [*Solomon*, 1971; *Redi*, 1982; *McDougall et al.*, 2014]. CM2.6 does not use parameterizations of the advective or diffusive transport due to mesoscale eddies; rather, both effects of eddies are at least partially represented through the resolved eddying flow.

3. Results

3.1. Hot spots of horizontal mass transport across the subtropical gyre boundaries

Mass and tracers may enter or leave the subtropical gyres at any point along the gyre boundaries. By examining the 10-year averaged transport of mass and tracers across the

subtropical gyre boundaries (hereafter cross-boundary transport) as a function of distance around the gyre, we first aim to shed light on hot spots of exchange and their associated physical mechanisms.

Figure 5 shows the 10-year averaged cumulative sum of the total, mean, and eddy mass and tracer cross-boundary transports into the subtropical gyre for each basin. The figure was constructed by taking the cumulative sum of the cross-boundary transport at each 0.1° longitude, starting from the western edge of the gyre boundary at 25°N for the North Pacific and 30°N for the North Atlantic and moving in the clockwise direction. 120°W (North Pacific) and 30°W (North Atlantic) correspond to the easternmost extent of the gyre; the boundary only extends this far east for a couple of months of the year (see Figure 2), so that the curves appear flat around these longitudes for the months when the gyre does not extend that far (not shown). The Kuroshio and Gulf Stream regions are labelled "jet", and the northern and southern gyre boundaries are labelled for transport occurring to the north and south of 25°N for North Pacific and 30°N for North Atlantic (see Figure 4a and b for mean boundary locations). The annual-mean is then weighted by the fraction of the year that the quasi-stream function is located at each longitude.

The figure shows that the total mass transport (first row in Figure 5) is inward in most places across the gyre boundaries integrated over the ventilated pycnoclines (defined in Section 2.2.2) for both of the basins. Inward mass transport is an expected consequence of the large-scale wind stress that causes subtropical convergence and downwelling. This inward transport is dominantly set by the mean transport, consistent with monthly-mean negative wind stress curl and convergent Ekman transport over the entire annual cycle (not shown). The vertical profile of the cross-boundary transport (Figure 6) reveals that

this inward transport occurs principally in the upper layer, above $\sigma_\theta = 23.5$ in North Pacific and $\sigma_\theta = 26.2$ in North Atlantic, further supporting the idea that the Ekman transport is the critical inward transport mechanism.

There is intense cross-boundary mass transport across the Kuroshio and Gulf Stream, accounting for 57% and 82% of the total mass transport, respectively. A comparison of the longitudes where cross-boundary transport is strongest in Figure 5 to the jet meander locations in Figure 2 reveals that the mean cross-jet transport is closely correlated with the curvature of the meandering of the jet system. Cyclonic curvatures in Kuroshio (e.g. at 133°E) and Gulf Stream correspond to peaks of inflowing mass, whereas the locations of anticyclonic curvatures correspond to local minima of the inflowing mass (e.g. at around 138°E). This result that the quasi-stationary meanders in the Kuroshio and Gulf Stream appear to be a hotspot for exchange in the model is in line with theoretical and observational studies [e.g. *Bower and Rossby*, 1989; *Bower*, 1991; *Sainz-Trápaga and Sugimoto*, 2000]. By analyzing the Lagrangian potential vorticity balance along a Kuroshio meander, *Sainz-Trápaga and Sugimoto* [2000] suggested that the cross-frontal transport associated with the curvature of the jet occurs due to the conservation of the potential vorticity of the water particles. As the water particles flow downstream in the jet, their planetary vorticity and curvature vorticity experience changes. These changes need to be compensated by changing horizontal velocity shear and/or layer thickness in order to conserve potential vorticity, which in turn results in anomalous cross-stream movement of the water particles. More specifically, in approaching cyclonic curvature, the water particles tend to flow towards the area with lower velocity shear and/or higher layer thickness,

inducing anomalous inflowing mass to the subtropical gyre, and vice versa for anticyclonic curvature.

The spatial patterns of cross-boundary transport are associated with well-known oceanographic features, even outside the jet regions. In the North Pacific, approximately 5 Sv of mass is transported into the gyre across its southern gyre boundary, which is almost entirely driven by the mean component. This large mass input likely arises from the persistent alignment of the location of the monthly southern gyre boundary in the low latitudes (see Figure 2) with the prevailing easterly winds, which drive mass input by Ekman transport. This pronounced mass input is followed by a dramatic mass export at around between 120°E and 130°E, acting to cancel approximately all the mass transported across the southern gyre boundary. The location where mass is exported from the subtropical gyre coincides with the location where Kuroshio intrudes into the South China Sea through Luzon Strait [*Nan et al.*, 2015], as well as where the westward North Equatorial Current, which constitutes the southern gyre boundary of the North Pacific subtropical gyre, reaches the Philippine coast and bifurcates into the northward Kuroshio and the southward Mindanao Current [*Qiu and Lukas*, 1996]. We therefore hypothesize that the large leakage of mass at this location is due to the divergence of the flows associated with the bifurcation of the North Equatorial Current as well as Kuroshio intrusion through Luzon Strait. In the North Atlantic, the mean mass transport across the southern gyre boundary is more uniform, and accounts for 18% of the total mass input into the gyre basin.

In both gyres, the most pronounced eddy mass transport is found in the jet regions, as is to be expected from the enhanced mesoscale activity there. Much of this mesoscale

transport, however, does not contribute to the net mass convergence or divergence, presumably due to the large rotational component of mass fluxes. The rotational component circulates around the eddy potential energy contours, and it does not contribute to the divergence of advective fluxes [*Marshall and Shutts*, 1981; *Bishop et al.*, 2013]. Although any advective flux consists of rotational and divergent components, no unique method exists for decomposing advective fluxes into these components [*Fox-Kemper et al.*, 2003]. The effect of the rotational component of the advective flux, nonetheless, vanishes for the sum of these fluxes around the closed contour encircling the gyre, leaving only the divergent component [*Dufour et al.*, 2015]. After summing around the entire gyre boundary, the average eddy mass transport is slightly negative (i.e. outward), which is in line with expectations that the mass export by the eddy component opposes the wind-driven time-mean flow, as discussed in Section 2.3. However, the eddy-driven mass transport is so small that it is statistically indistinguishable from zero, after accounting for the interannual variability. The small outward eddy mass flux is due to transport near the base of the ventilated pycnocline, which competes with inward mass input on lighter layers (Figure 6).

In total, 10.2 Sv and 3.0 Sv of mass is imported across the gyre boundaries for the North Pacific and North Atlantic subtropical gyres, respectively. After normalization by the annual-mean gyre area (right axis on Figure 5), these transports are similar in magnitude, with the North Pacific gyre horizontally receiving 19.6 m yr^{-1} and the North Atlantic 17.8 m yr^{-1}. Following mass conservation, these values roughly correspond to mean downwelling, and they are within the expected range of Ekman downwelling in these subtropical gyre regions [Chapter 10 in *Marshall and Plumb*, 2007].

3.2. Relative roles of advection and down-gradient mixing in the supply of DIC, heat, and PO_4 to the subtropical gyres

The spatial pattern of mean- and eddy-driven DIC and heat transport resembles that of mass transport, as can be seen in Figure 5 and 6. This is not surprising, since the tracers are advected by the residual mean (or total mass) transport, which is the sum of mean and eddy advective mass transports. Therefore, in the absence of strong down-gradient, along-isopycnal tracer mixing, mass and tracer transport should follow similar patterns. The horizontal input of DIC and heat by the mean component into the subtropical gyre together reduces the capacity to take up atmospheric CO_2 in both gyres, given that cross-boundary input of DIC and heat increase the sea surface partial pressure of CO_2 (pCO_2) in the gyre [*Bates et al.*, 1998; *Takahashi et al.*, 2009; *Ayers and Lozier*, 2012]. Eddies act to remove 27% (31%) of the DIC supplied by the mean flow in the North Pacific (North Atlantic), and 13% (21%) of the heat. Much of this outward eddy transport occurs across the jets and the southern gyre boundaries of both gyres, near the base of the ventilated pycnocline. As was the case for the mass transport, roughly three times more DIC and heat are transported into the North Pacific subtropical gyre compared to the North Atlantic. After normalizing by the annual mean gyre area, these supply terms come to similar values for the Atlantic and Pacific (right axis on Figure 5).

In stark contrast, the eddy-driven transport of PO_4 is inward and makes up of the majority of the cross-boundary nutrient transport in both gyres, a behaviour that is unique among the tracers. The inward PO_4 transport by the eddy component explains 59% and 120% of the total transport of PO_4, for the North Pacific and the North Atlantic, respectively (in the North Atlantic the eddy supply is opposed by the mean, such that it

exceeds the total). This eddy-driven flux of PO_4 enters the subtropical gyre principally across the Kuroshio and Gulf Stream, and, to a lesser degree, over the southern gyre boundary in the North Pacific (Figure 5). Most of the eddy-driven supply occurs near the base of the ventilated pycnocline in both gyres (Figure 6). In the North Pacific, the mean component also supplies PO_4 into the subtropical gyre, while in the North Atlantic, the transport by the mean flow acts to remove PO_4 from the gyre, even while the mean supply of mass is inward. This difference in the role of the mean flow in the PO_4 budget between the gyre basins arises from the fact that the circulation at the base of the ventilated layer in the North Atlantic is flowing out of the gyre, whereas the North Pacific flow over the entire layer is inward, as can be seen from the vertical profile of the cross-boundary mass transport in Figure 6. Because the PO_4 at the base of the layer is elevated relative to the shallower depths where concentrations are essentially zero, this small outflow of the mean circulation at the base of the layer translates to an overall outward PO_4 transport due to the mean circulation.

As was briefly discussed in Section 2.3, the eddy-driven tracer transport that is not carried by the eddy mass transport can be explained by the down-gradient along-isopycnal tracer transport by the eddies, which arises due to the correlation between the velocity and tracer anomalies, $\bar{h}\overline{\mathbf{u}'C'}$. This down-gradient eddy transport of a tracer C, χ_C, across the gyre boundary on an isopycnal layer can be roughly scaled as follows [*Griffies*, 2004; *Dufour et al.*, 2015]:

$$\chi_C = -\rho_0 \kappa \bar{h} (\nabla \bar{C}) \cdot \hat{\mathbf{n}} dl, \tag{7}$$

where ρ_0 is a reference seawater density, $\kappa > 0$ is an along-isopycnal eddy diffusivity coefficient, h is the isopycnal layer thickness, dl is the segment of the gyre boundary,

and $\hat{\mathbf{n}}$ is the vector normal to dl. The eddy diffusivity coefficient, κ, is a function of space and time [e.g. *Ferrari and Nikurashin*, 2010], and its variations should be consistent across all tracers. CM2.6 resolves much of the mesoscale variability responsible for this down-gradient mixing in the subtropics, and includes no diffusive closure for such fluxes. Hence, we expect the magnitude of the tracer gradients to explain the difference between the importance for the eddy-driven PO_4 transport relative to that for DIC and heat.

Figure 7 shows the normalized 10-year averaged tracer gradient at every 0.1° longitude along the gyre boundary, with positive values indicating higher concentrations outside the gyre than inside. With this sign convention, down-gradient mixing along a positive gradient would provide a source of tracer to the subtropical gyre. The figure reveals that the strongest tracer gradients are found across the Kuroshio and Gulf Stream regions relative to the rest of the gyre boundary for all the tracers. It is also seen from the figure that the tracer gradient is positive for DIC and PO_4 (higher values outside the subtropical gyres), whereas it is dominantly negative for temperature (higher values inside the subtropical gyre), as expected from Figure 1. Therefore, down-gradient tracer mixing would supply DIC and PO_4 to the gyre, opposing the outward eddy mass transport, with the opposite effect for temperature, for which down-gradient mixing would augment the outward eddy mass temperature transport. In spite of this expectation, there is no obvious difference in the spatial pattern of the cumulative eddy transport of DIC, heat, and mass across the gyre boundary in Figure 5 and 6. Part of the reason for the similarity in spatial structure of the eddy fluxes for DIC and mass is that the gradients in DIC concentration across the gyre margins are relatively subdued compared to the other tracers, since DIC variations are small relative to background concentrations ($>$ 1,800

μmol kg^{-1} everywhere in the ocean, as simulated under preindustrial atmospheric CO_2; see Figure 1). Thus, the eddy advective transport likely dominates the small magnitude of the down-gradient diffusive transport for DIC. The similarity in the spatial pattern between the eddy-driven cumulative flux of mass and temperature, despite the potential role of down-gradient mixing to augment the role of the eddy mass transport, may suggest that the eddies acting to smooth thickness gradients and tracer gradients have a similar spatial distribution.

The fact that the eddy-induced transport is outward across gyre boundaries for DIC and temperature and inward for PO_4 is in line with the results of *Lee and Williams* [2000], who suggested that the eddy advective transport dominates over the down-gradient diffusive transport for long-lived tracers like DIC and temperature. In contrast, since PO_4 is a short-lived tracer due to its rapid biological drawdown in the near-surface layer, the eddy-driven diffusive transport dominates over the eddy advective transport. As a consequence of being a short lived tracer, the normalized PO_4 gradient becomes heightened to approximately 1.5 times larger than the normalized DIC gradient for the North Pacific and nearly 20 times larger in the North Atlantic on average. The down gradient mixing across this stark biogeochemical divide drives a major nutrient supply to the subtropical gyre.

The PO_4 gradient across the Kuroshio and Gulf Stream is sharper than the temperature and DIC gradients because PO_4 concentrations are drawn down to near-zero on the subtropical side of the boundary currents almost to the base of the ventilated layer. Here, light does not seem to limit productivity, as phytoplankton bloom during deep mixing in the darkest months of winter [*Palter et al.*, 2005]. Iron is also relatively abundant, partic-

ularly in the North Atlantic, permitting complete PO_4 depletion [*Mahowald et al.*, 2005; *Sedwick et al.*, 2005]. The PO_4-depleted water masses formed just south of the jet regions are subducted as STMW and recirculate well below the euphotic zone south of their formation region. Therefore, PO_4 is restored on those layers via remineralization [*Palter et al.*, 2005]. These layers rejoin the Gulf Stream and Kuroshio, where they are swiftly transported in what has been referred to as a "nutrient stream" [*Pelegri and Csanady*, 1991; *Williams et al.*, 2006; *Palter and Lozier*, 2008; *Guo et al.*, 2012]. Thus, the stark nutrient gradients across the Kuroshio and Gulf Stream are sustained by the presence of these nutrient streams and the depletion of the nutrient just south of the boundary currents. Finally, unlike DIC and temperature, PO_4 is not subject to air-sea flux exchange, which tends to smooth out horizontal tracer gradients.

It is also noteworthy that the cross-boundary PO_4 flux is nearly twice as large in the North Atlantic subtropical gyre as the North Pacific after normalizing by gyre area, as can be seen in the right axis on Figure 5. In contrast, mass, heat and DIC cross-boundary transport per unit area is similar for both gyres. This difference between the two gyres likely stems from the fact that in the Gulf Stream, unlike in the Kuroshio, nutrient concentrations are further enriched by waters imported from outside the subtropical gyre, such as from the tropics and Southern Ocean, in the shallow return pathway of the Atlantic Meridional Overturning Circulation [*Palter and Lozier*, 2008]. As a result, the nutrient transport along the Gulf Stream is approximately 4 - 5 times larger compared to the Kuroshio [*Guo et al.*, 2012], leading to the sharper PO_4 gradient across the Gulf Stream than across the Kuroshio. In addition, the gyre-to-gyre difference may be further enhanced by the greater availability of iron in subtropical North Atlantic due to atmo-

spheric deposition of iron-rich Saharan dust [*Mahowald et al.*, 2005; *Sedwick et al.*, 2005]. Iron is an important limiting nutrient, and the difference in the iron availability between the basins likely leads to a more complete PO_4 drawdown in the North Atlantic subtropical gyre [*Wu et al.*, 2000] and a sharper PO_4 gradient at its boundaries, compared to its North Pacific counterpart.

3.3. Importance of the cross-boundary tracer transports for the subtropical gyre budgets

Finally, the importance of the cross-boundary transport is evaluated by performing an annual budget analysis over the gyre regions (Figure 8). Both DIC and heat are almost exclusively supplied by the mean component of the horizontal transport across the gyre boundary. The eddies oppose the mean transport, removing about a third of the DIC and a quarter of the heat from both the North Atlantic and North Pacific gyres. Two thirds of the DIC horizontally supplied downwells, as expected from the large scale downwelling in the subtropical gyre regions, with the air-sea exchange of carbon as well as the biological consumption and remineralization of DIC playing only very minor roles. We remind the reader that this simulation is run with a preindustrial atmospheric CO_2 concentration, and does not include the anthropogenic rise in CO_2. Heat is lost from both subtropical gyres to the atmosphere at a rate greater than 30 W m^{-2}, which is the same order of magnitude as the heat export by the eddy component and the downwelling. As noted earlier, the supply of PO_4 is dominantly set by the eddy component of cross-boundary horizontal transport for both gyres, but particularly so for the North Atlantic. The total horizontal transport, combining the roles of both mean and eddy components, makes up 77% of the total nutrient supply in the North Pacific and 86% in the North Atlantic. These values

are roughly 1.5 times larger than the estimate by *Letscher et al.* [2016], who evaluated the horizontal supply of nutrients in a data-constrained, coarse-resolution ocean model, using fixed horizontal subtropical gyre boundaries and the fixed local annual maximum mixed layer depth as the vertical limit. It is unclear if the source of this difference arises from differences in the simulated PO_4 gradients, differences in the definition of the gyre boundaries, and/or the fact that our simulation resolves a large spectrum of mesoscale fluctuations that were parameterized in the simulations of *Letscher et al.* [2016]. In any case, both studies agree that the supply of nutrients to the subtropical gyres is largely governed by horizontal exchange across its boundaries, despite important differences in the model used to evaluate the supply and distinct definitions of gyre boundaries.

4. Discussion and Conclusions

In this study, we have investigated the role of the mesoscale eddies in the transport of mass, heat, carbon, and nutrients into the North Pacific and North Atlantic subtropical gyres over the annual-mean timescale, in a preindustrial simulation of an eddy-rich climate model coupled to a simplified biogeochemistry model (CM2.6-miniBLING). We proposed a new gyre boundary definition based on a combination of dynamical and property-based criteria. The horizontal gyre boundaries are defined by the largest region of anticyclonic circulation, whereas the vertical extent is set by the isopycnal that underlies a pool of warm, oxygenated, oligotrophic water, which we call the ventilated pycnocline following *Luyten et al.* [1983]. The transport across the subtropical gyre boundary thus defined was decomposed into a mean component and a mesoscale eddy component following *Griffies et al.* [2015] and *Dufour et al.* [2015].

A schematic summary of the transport of mass and each tracer is shown in Figure 9. Mass, heat, and DIC supply into the gyres are mainly set by the mean component of the transport. The concurrent transport of heat and DIC together act to reduce the subtropical ocean uptake of atmospheric CO_2 below what it would be in the absence of such horizontal exchange, by increasing the pCO_2 in the subtropical seawater. Mesoscale eddies tend to remove mass, heat and DIC supplied by the mean component from the gyres. This cancellation of the mean circulation by the eddy-driven circulation is in line with the expected role of baroclinic eddies in flattening isopycnals, which are steepened by the time-mean, wind-driven circulation [*Gent and McWilliams*, 1990], and agrees with previous studies evaluating tracer budgets using the same model [*Griffies et al.*, 2015; *Dufour et al.*, 2015].

Transport of PO_4 differs markedly from mass and the other tracers, in that the eddies are the primary supply mechanism of PO_4 into the subtropical gyres of both basins. We attribute this greater role for the eddies to the sharp PO_4 gradients across the gyre boundaries, which allow for strong down-gradient mixing. The effect of the outward eddy-induced mass transport on PO_4 transport is, thus, seemingly swamped by the down-gradient PO_4 diffusive transport. In turn, the strong PO_4 gradient across the Gulf Stream and Kuroshio relative to the other tracers is interpreted as a consequence of biological activity. PO_4 serves as a limiting nutrient for primary productivity in the subtropical gyre regions, resulting in the near-complete depletion of PO_4 to the base of the subtropical euphotic zone or mixed layer, whichever is deeper. On isopycnals beneath the euphotic zone or mixed layer, nutrients are restored via remineralization during recirculation before rejoining the Kuroshio and Gulf Stream. Because the deepest mixed layers are formed just

south of the Gulf Stream and Kuroshio, the largest nutrient gradients are found across these jets. Our results agree with inferences from a previous study by *Lee and Williams* [2000], who used an idealized model to illustrate that down-gradient eddy diffusive transport should play the leading role over eddy advection for tracers with a short lifetime, such as PO_4, which is rapidly consumed by photosynthesis in the subtropics.

Budget analysis reveals that horizontal cross-boundary transport supplies the major fraction of mass, heat, DIC, and PO_4 to the subtropical gyre regions in both the North Pacific and the North Atlantic basins on an annual-mean basis. Approximately one third of DIC supplied to the subtropical gyres primarily by the mean component is removed by the eddy horizontal transport on an annual-mean basis, while the rest downwells. Although today's subtropical gyres are important uptake regions for CO_2 [*Takahashi et al.*, 2009], the air-sea exchange of carbon contributes little to the subtropical carbon budget in both basins in this preindustrial model simulation. On the other hand, the heat sink balancing the cross-boundary supply by the mean flow is approximately equally split between removal by eddies, ocean to atmosphere heat loss, and downwelling. Horizontal PO_4 input is the dominant nutrient source to both subtropical gyres, amounting to 77% of the total nutrient supply in the North Pacific and 86% in the North Atlantic, with the remaining supply due to vertical mixing. Given that the observed dynamical sea level variance at the Gulf Stream in satellite altimetry is higher than the simulated variance as briefly discussed in Section 2.1, we speculate that these eddy fluxes diagnosed from the model may be lower than what occurs in reality. Our study agrees with previous work that underscored the importance of the horizontal nutrient supply into the subtropical gyres [e.g. *Letscher et al.*, 2016], and shows this qualitative result is not sensitive to the model

used to estimate the horizontal fluxes or the boundaries drawn around the gyres. Our study therefore further highlights the need for Earth system models and climate models to adequately represent such horizontal transport to the subtropical gyres. Accurate simulation of the horizontal transport is especially critical, provided that the increased vertical stratification under the ongoing climate change could further suppress the vertical nutrient supply [e.g., *Fu et al.*, 2016]. Under such a circumstance, the supply mechanism of the nutrients to the subtropical gyres may shift such that the horizontal transport of nutrients plays an even greater role in gyre productivity [*Letscher et al.*, 2016], although careful evaluations are required to validate such a regime shift.

In addition, our work also examined the spatial pattern of the tracer exchange and the mechanisms by which the tracers enter the gyre, which point towards a critical role for the horizontal exchange across the Kuroshio and Gulf Stream in supplying a large quantity of tracers to the northern fringe of the gyres. We further found that the mean component of the cross-jet transport is closely associated with quasi-stationary jet meanders. Cyclonic jet meanders create hot spots for inward transport of mass and tracer to the subtropical gyre, while anticyclonic jet meanders favour outward transport, consistent with previous observational and theoretical studies [e.g. *Bower and Rossby*, 1989; *Bower*, 1991; *Sainz-Trápaga and Sugimoto*, 2000]. This aspect of our results indicates that anticyclonic curvature of the western boundary current tends to transport carbon, heat, and nutrients towards coastal areas, thus having an important implication for the shelf fisheries.

It is tempting to attribute the differences between the results from our analysis with the use of a high resolution model and the results from the previous studies using non-eddy resolving models to the difference in the model resolutions. However, there are so many

differences between the coarse resolution models previously analyzed and CM2.6 that it is not appropriate to make inferences about the role of the parameterizations in causing the differences. Instead, our study reveals the role of eddies when they are resolved, thereby including dynamics that are typically excluded from eddy parameterizations, such as spatial and temporal variability in the effective turbulent diffusivity (particularly as a function of depth) and the role of meanders in creating hot-spots of exchange mentioned in the previous paragraph.

These results summarized above are qualitatively robust and insensitive to the values of the streamfunction one uses to define the horizontal extent of the gyre, so long as the definition of the subtropical gyres is dynamical and the western edges are aligned with the western boundary currents, as described in Section 2.2.1. This agreement stems from the fact that the jet region is where most of the cross-boundary flux occurs, as can be seen in Figure 5. By definition, the jet is a region where streamlines are tightly packed. Thus, opting for slightly different values of streamfunctions to define the gyre barely changes the position of the boundary in the jet region, and the overall flux across the jet is not sensitive to this choice. While choosing a different streamline could lead to distinct boundary positions in the open gyre region, the cross-boundary fluxes are so small here, that the net cross-boundary flux is changed by a very small amount (not shown).

In the current study, we have applied the standard Reynold's decomposition for the temporal field in order to partition mesoscale eddies from the mean component. While this method is used extensively in previous studies [e.g., *McGillicuddy Jr. et al.*, 2003; *Griffies et al.*, 2015; *Dufour et al.*, 2015], we fully acknowledge that there are various metrics to define oceanic mesoscale eddies, including implementation of the spatial filtering

[e.g., *Qiu and Chen*, 2005] and detection and tracking of the mesoscale coherent vortices [e.g., *Faghmous et al.*, 2015]. Whether utilizing different mesoscale eddy definitions in our analysis would lead to similar conclusions is an intriguing question, which remains to be addressed in the future studies.

In summary, our results confirm the importance of horizontal transport in the tracer budgets of the Northern Hemisphere subtropical gyres. It is notable that the majority of PO_4 that fuels new primary productivity is provided by horizontal transport across the Kuroshio and Gulf Stream, with eddies being the principal supply mechanism. Another important result of this work is that cross-boundary transport provides the primary source of heat to the gyre on an annual basis; some of this heat is removed by eddies and downwelling, while roughly a third is lost to the overlying atmosphere. Given the first-order role of cross-boundary fluxes in the upper-ocean heat budget, we expect these transport processes to be critical to restratification of the subtropical mode waters, with the potential to influence the subduction of thermal anomalies that give memory to the climate system.

Acknowledgments. We would like to thank J. Gyakum, T. Merlis, B. Winter, B. Dong, C. Stock, M. Nonaka, T. Ogata, T. Hihara, N. Yoshie and three anonymous reviewers for their constructive comments and discussions which greatly improved the earlier versions of this manuscript. Funding for this study was received from the Natural Sciences and Engineering Research Council of Canada (NSERC) Discovery program. C. O. Dufour was supported by the National Aeronautics and Space Administration (NASA) under Award NNX14AL40G and by the Princeton Environmental Institute (PEI) Grand Challenge Initiative. The observational fields of temperature, PO_4, NO_3

and O_2 were obtained from the World Ocean Atlas 2009 [*Locarnini et al.*, 2010; *Garcia et al.*, 2010a, b] (`https://www.nodc.noaa.gov/OC5/WOA09/pr_woa09.html`). The observed DIC field corrected to preindustrial values was retrieved from GLODAP [*Key et al.*, 2004] (`http://cdiac.ornl.gov/oceans/glodap/`), and the observed SSH field was obtained from AVISO [*Ducet et al.*, 2000] (`https://www.aviso.altimetry.fr`).

References

Alexander, M. A., and C. Deser (1995), A Mechanism for the recurrence of wintertime midlatitude SST anomalies, *Journal of Physical Oceanography*, *25*, 122–137.

Ayers, J. M., and M. S. Lozier (2010), Physical controls on the seasonal migration of the North Pacific transition zone chlorophyll front, *Journal of Geophysical Research*, *115*, C05,001, doi:10.1029/2009JC005596.

Ayers, J. M., and M. S. Lozier (2012), Unraveling dynamical controls on the North Pacific carbon sink, *Journal of Geophysical Research*, *117*, C01,017, doi:10.1029/2011JC007368.

Bates, N. R., T. Takahashi, D. W. Chipman, and A. H. Knap (1998), Variability of pCO_2 on diel to seasonal timescales in the Sargasso Sea near Bermuda, *Journal of Geophysical Research*, *103*, 15,567–15,585.

Bishop, S. P., D. R. Watts, and K. A. Donohue (2013), Divergent Eddy Heat Fluxes in the Kuroshio Extension at 144-148E. Part I: Mean Structure, *Journal of Physical Oceanography*, *43*, 1533–1550, doi:10.1175/JPO-D-12-0221.1.

Bower, A. S. (1991), A Simple Kinematic Mechanism for Mixing Fluid Parcels across a Meandering Jet, doi:10.1175/1520-0485(1991)021⟨0173:ASKMFM⟩2.0.CO;2.

Bower, A. S., and T. Rossby (1989), Evidence of Cross-Frontal Exchange Processes in the Gulf Stream Based on Isopycnal RAFOS Float Data, *Journal of Physical Oceanography*, *19*, 1177–1190, doi:10.1175/1520-0485(1989)019⟨1177:EOCFEP⟩2.0.CO;2.

Bower, A. S., H. T. Rossby, and J. L. Lillibridge (1985), The Gulf Stream-barrier or blender?, *Journal of Physical Oceanography*, *15*, 24–32.

Cassou, C., C. Deser, and M. A. Alexander (2007), Investigating the Impact of Reemerging Sea Surface Temperature Anomalies on the Winter Atmospheric Circulation over the North Atlantic, *Journal of Climate*, *20*(14), 3510–3526, doi:10.1175/JCLI4202.1.

Delworth, T. L., A. Rosati, W. Anderson, A. J. Adcroft, V. Balaji, R. Benson, K. Dixon, S. M. Griffies, H.-C. Lee, R. Pacanowski, G. A. Vecchi, A. T. Wittenberg, F. Zeng, and R. Zhang (2012), Simulated Climate and Climate Change in the GFDL CM2.5 High-Resolution Coupled Climate Model, *Journal of Climate*, *25*, 2755–2781, doi:10.1175/JCLI-D-11-00316.1.

Dong, C., J. C. McWilliams, Y. L. Liu, and D. Chen (2014), Global heat and salt transports by eddy movement, *Nature Communications*, *5*.

Ducet, N., P. Y. Le Traon, and G. Reverdin (2000), Global high-resolution mapping of ocean circulation from TOPEX/Poseidon and ERS-1 and -2, *J. Geophys. Res.*, *105*, 19,477–19,498.

Dufour, C., S. M. Griffies, A. K. Morrison, J. B. Palter, J. L. Sarmiento, E. D. Galbraith, J. P. Dunne, W. G. Anderson, and R. D. Slater (2015), Role of mesoscale eddies in cross-frontal transport of heat and biogeochemical tracers in the Southern Ocean, *Journal of Physical Oceanography*, *45*, 3057–3081.

Faghmous, J. H., I. Frenger, Y. Yao, R. Warmka, A. Lindell, and V. Kumar (2015), A daily global mesoscale ocean eddy dataset from satellite altimetry, *Scientific Data*, *2*, 150,028, doi:10.1038/sdata.2015.28.

Ferrari, R., and M. Nikurashin (2010), Suppression of Eddy Diffusivity across Jets in the Southern Ocean, *Journal of Physical Oceanography*, *40*, 1501–1519, doi:10.1175/2010JPO4278.1.

Fox-Kemper, B., R. Ferrari, and J. Pedlosky (2003), On the Indeterminacy of Rotational and Divergent Eddy Fluxes, *Journal of Physical Oceanography*, *33*, 478–483.

Fox-Kemper, B., G. Danabasoglu, R. Ferrari, S. M. Griffies, R. W. Hallberg, M. M. Holland, M. E. Maltrud, S. Peacock, and B. L. Samuels (2011), Parameterization of mixed layer eddies. III: Implementation and impact in global ocean climate simulations, *Ocean Modelling*, *39*, 61–78, doi:10.1016/j.ocemod.2010.09.002.

Fratantoni, D. M. (2001), North atlantic surface circulation during the 1990's observed with satellite-tracked drifters, *Journal of Geophysical Research: Oceans*, *106*(C10), 22,067–22,093, doi:10.1029/2000JC000730.

Fu, W., J. T. Randerson, and J. Keith Moore (2016), Climate change impacts on net primary production (NPP) and export production (EP) regulated by increasing stratification and phytoplankton community structure in the CMIP5 models, *Biogeosciences*, *13*(18), 5151–5170, doi:10.5194/bg-13-5151-2016.

Galbraith, E. D., and A. C. Martiny (2015), A simple nutrient-dependence mechanism for predicting the stoichiometry of marine ecosystems, *PNAS*, *112*, 8199–8204.

Galbraith, E. D., A. Gnanadesikan, J. P. Dunne, and M. R. Hiscock (2010), Regional impacts of iron-light colimitation in a global biogeochemical model, *Biogeosciences*, *7*,

1043–1064.

Galbraith, E. D., J. P. Dunne, A. Gnanadesikan, D. Richard, J. L. Sarmiento, C. O. Dufour, G. F. De Souza, D. Bianchi, M. Claret, K. B. Rodgers, and S. S. Marvasti (2015), Complex functionality with minimal computation: Promise and pitfalls of reduced-tracer ocean biogeochemistry models, *Journal of Advances in Modeling Earth Systems*, *7*, 2012–2028.

Garcia, H. E., R. A. Locarnini, T. P. Boyer, J. I. Antonov, M. M. Zweng, O. K. Baranova, and D. R. Johnson (2010a), Volume 4: Nutrients (phosphate, nitrate, silicate), in *WORLD OCEAN ATLAS 2009*, edited by S. Levitus, p. 398 pp., NOAA Atlas NESDIS 71, U.S. Government Printing Office, Washington, D. C.

Garcia, H. E., R. A. Locarnini, T. P. Boyer, J. I. Antonov, O. K. Baranova, M. M. Zweng, and D. R. Johnson (2010b), Volume 3: Dissolved Oxygen, Apparent Oxygen Utilization, and Oxygen Saturation, in *WORLD OCEAN ATLAS 2009*, edited by S. Levitus, p. 344 pp., NOAA Atlas NESDIS 70, U.S. Government Printing Office, Washington, D. C.

Gent, P. R., and J. C. McWilliams (1990), Isopycnal mixing in ocean circulation models, *Journal of Physical Oceanography*, *20*, 150–155.

Gent, P. R., J. Willebrand, T. J. McDougall, and J. C. McWilliams (1995), Parameterizing Eddy-Induced Tracer Transports in Ocean Circulation Models, *Journal of Physical Oceanography*, *25*, 463–474.

Griffies, S. M. (2004), *Fundamentals of Ocean Climate Models*, 518 pp., Princeton University Press, Princeton, NJ.

Griffies, S. M. (2012), Elements of the Modular Ocean Model (MOM), *Tech. rep.*, NOAA/Geophysical Fluid Dynamics Laboratory, Princeton, NJ.

Griffies, S. M., M. Winton, W. G. Anderson, R. Benson, T. L. Delworth, C. O. Dufour, J. P. Dunne, P. Goddard, A. K. Morrison, A. Rosati, A. T. Wittenberg, J. Yin, and R. Zhang (2015), Impacts on Ocean Heat from Transient Mesoscale Eddies in a Hierarchy of Climate Models, *Journal of Climate*, *28*, 952–977, doi: 10.1175/JCLI-D-14-00353.1.

Guo, X., X.-H. Zhu, Q.-S. W. Wu, and D. Huang (2012), The Kuroshio nutrient stream and its temporal variation in the East China Sea, *Journal of Geophysical Research*, *117*, C01,026.

Hallberg, R. (2013), Using a resolution function to regulate parameterizations of oceanic mesoscale eddy effects, *Ocean Modelling*, *72*, 92–103, doi:10.1016/j.ocemod.2013.08.007.

Hanawa, K., and L. D. Talley (2001), Mode Waters, in *Ocean Circulation and Climate*, edited by G. Siedler and J. Church, chap. 5.4, pp. 373–386, Academic Press.

Huang, R. X., and B. Qiu (1994), Three-Dimensional Structure of the Wind-Driven Circulation in the Subtropical North Pacific, *Journal of Physical Oceanography*, *24*, 1608–1622.

Irwin, A. J., and M. J. Oliver (2009), Are ocean deserts getting larger ?, *Geophysical Research Letters*, *36*, L18,609, doi:10.1029/2009GL039883.

Key, R. M., A. Kozyr, C. L. Sabine, K. Lee, R. Wanninkhof, J. L. Bullister, R. A. Feely, F. J. Millero, C. Mordy, and T. Peng (2004), A global ocean carbon climatology: Results from Global Data Analysis Project (GLODAP), *Global Biogeochemical Cycles*, *18*, GB4031, doi:10.1029/2004GB002247.

Kwon, E. Y., Y. H. Kim, Y.-G. Park, Y.-H. Park, J. P. Dunne, J. L. Sarmiento, and K.-I. Chang (2016), Multi-decadal Wind-Driven Shifts in Northwest Pacific Temperature,

Salinity, O2 and PO4, *Global Biogeochemical Cycles*.

Kwon, Y.-O., M. A. Alexander, N. A. Bond, C. Frankignoul, H. Nakamura, B. Qiu, and L. Thompson (2010), Role of the gulf Stream and Kuroshio-Oyashio systems in large-scale atmosphere-ocean interaction: A review, *Journal of Climate*, *23*, 3249–3281, doi:10.1175/2010JCLI3343.1.

Large, W. G., J. C. McWilliams, and S. C. Doney (1994), Oceanic Vertical Mixing: A Review and a Model with a Nonlocal Boundary Layer Parameterization, *Reviews of Geophysics*, pp. 363–403.

Lee, H.-C., A. Rosati, and M. J. Spelman (2006), Barotropic tidal mixing effects in a coupled climate model: Oceanic conditions in the Northern Atlantic, *Ocean Modelling*, *11*, 464–477, doi:10.1016/j.ocemod.2005.03.003.

Lee, M.-M., and R. G. Williams (2000), The role of eddies in the isopycnic transfer of nutrients and their impact on biological production, *Journal of Marine Research*, *58*, 895–917, doi:10.1357/002224000763485746.

Letscher, R. T., F. Primeau, and J. K. Moore (2016), Nutrient budgets in the subtropical ocean gyres dominated by lateral transport, *Nature Geoscience*, *9*, 815–819, doi:10.1038/NGEO2812.

Locarnini, R. A., A. V. Mishonov, J. I. Antonov, T. P. Boyer, H. E. Garcia, O. K. Baranova, M. M. Zweng, and D. R. Johnson (2010), Volume 1: Temperature, in *WORLD OCEAN ATLAS 2009*, edited by S. Levitus, p. 184, NOAA Atlas NESDIS 68, U.S. Government Printing Office, Washington, D. C.

Lozier, M. S., A. C. Dave, J. B. Palter, L. M. Gerber, and R. T. Barber (2011), On the relationship between stratification and primary productivity in the North Atlantic,

Geophysical Research Letters, *38*, L18,609, doi:10.1029/2011GL049414.

Luyten, J. R., J. Pedlosky, and H. Stommel (1983), The Ventilated Thermocline, *Journal of Physical Oceanography*, *13*, 292–309.

Mahowald, N. M., A. R. Baker, G. Bergametti, N. Brooks, R. A. Duce, T. D. Jickells, N. Kubilay, J. M. Prospero, and I. Tegen (2005), Atmospheric global dust cycle and iron inputs to the ocean, *Global Biogeochemical Cycles*, *19*, GB4025, doi:10.1029/2004GB002402.

Marshall, J., and R. A. Plumb (2007), *Atmosphere, Ocean and Climate Dynamics: an Introductory Text*, 1 ed., Academic Press, Burlington, MA, USA.

Marshall, J., and G. Shutts (1981), A Note on Rotational and Divergent Eddy Fluxes, *Journal of Physical Oceanography*, *11*, 1677–1680.

Masuzawa, J. (1969), Subtropical Mode Water, *Deep-Sea Research*, *16*, 463–472.

McClain, C. R., S. R. Signorini, and J. R. Christian (2004), Subtropical gyre variability observed by ocean-color satellites, *Deep Sea Research Part II: Topical Studies in Oceanography*, *51*, 281–301, doi:10.1016/j.dsr2.2003.08.002.

McDougall, T. J., S. Groeskamp, and S. M. Griffies (2014), On Geometrical Aspects of Interior Ocean Mixing, *Journal of Physical Oceanography*, *44*, 2164–2175, doi:10.1175/JPO-D-13-0270.1.

McGillicuddy Jr, D. J., A. R. Robinson, D. A. Siegel, H. W. Jannasch, R. Johnson, T. D. Dickey, J. McNeil, A. F. Michaels, and A. H. Knap (1998), Influence of mesoscale eddies on new production in the Sargasso Sea, *Nature*, *394*, 263–266.

McGillicuddy Jr., D. J., L. A. Anderson, S. C. Doney, and M. E. Maltrud (2003), Eddy-driven sources and sinks of nutrients in the upper ocean: Results from a 0.1° resolution

model of the North Atlantic, *Global Biogeochemical Cycles*, *17*(2), 1035, doi:10.1029/2002GB001987.

Nan, F., H. Xue, and F. Yu (2015), Kuroshio intrusion into the South China Sea: A review, *Progress in Oceanography*, *137*, 314–333, doi:10.1016/j.pocean.2014.05.012.

Nicholson, D., S. Emerson, and C. C. Eriksen (2008), Net community production in the deep euphotic zone of the subtropical North Pacific gyre from glider surveys, *Limnology and Oceanography*, *53*, 2226–2236.

Oka, E., B. Qiu, Y. Takatani, K. Enyo, D. Sasano, N. Kosugi, M. Ishii, T. Nakano, and T. Suga (2015), Decadal variability of Subtropical Mode Water subduction and its impact on biogeochemistry, *Journal of Oceanography*, doi:10.1007/s10872-015-0300-x.

Omand, M. M., and A. Mahadevan (2015), The shape of the oceanic nitracline, *Biogeosciences*, *12*, 3273–3287, doi:10.5194/bg-12-3273-2015.

Oschlies, A. (2002), Nutrient supply to the surface waters of the North Atlantic: A model study, *Journal of Geophysical Research*, *107*(C5), 3046.

Oschlies, A., and V. Garçon (1998), Eddy-induced enhancement of primary production in a model of the North Atlantic Ocean, *Nature*, *394*(July), 266–269.

Palter, J. B., and M. S. Lozier (2008), On the source of Gulf Stream nutrients, *Journal of Geophysical Research*, *113*, C06,018, doi:10.1029/2007JC004611.

Palter, J. B., M. S. Lozier, and R. T. Barber (2005), The effect of advection on the nutrient reservoir in the North Atlantic subtropical gyre, *Nature*, *437*, 687–692, doi:10.1038/nature03969.

Palter, J. B., M. S. Lozier, J. L. Sarmiento, and R. G. Williams (2011), The supply of excess phosphate across the Gulf Stream and the maintenance of subtropical nitrogen

fixation, *Global Biogeochemical Cycles*, *25*, doi:10.1029/2010GB003955.

Palter, J. B., I. Marinov, J. L. Sarmiento, and N. Gruber (2013), Large-Scale, Persistent Nutrient Fronts of the World Ocean: Impacts on Biogeochemistry, in *Chemical Oceanography of Frontal Zones*, edited by I. M. Belkin, Springer, Berlin, doi:10.1007/698.

Pelegri, J. L., and G. T. Csanady (1991), Nutrient transport and mixing in the Gulf Stream, *Journal of Geophysical Research*, *96*, 2577–2583.

Qiu, B., and S. Chen (2005), Eddy-Induced Heat Transport in the Subtropical North Pacific from Argo, TMI, and Altimetry Measurements, *Journal of Physical Oceanography*, *35*(4), 458–473, doi:10.1175/JPO2696.1.

Qiu, B., and S. Chen (2006), Decadal Variability in the Formation of the North Pacific Subtropical Mode Water: Oceanic versus Atmospheric Control, *Journal of Physical Oceanography*, *36*, 1365–1380, doi:10.1175/JPO2918.1.

Qiu, B., and R. Lukas (1996), Seasonal and interannual variability of the North Equatorial Current, the Mindanao Current, and the Kuroshio along the Pacific western boundary, *Journal of Geophysical Research*, *101*, 12,315–12,330.

Qiu, B., S. Chen, and P. Hacker (2007), Effect of Mesoscale Eddies on Subtropical Mode Water Variability from the Kuroshio Extension System Study (KESS), *Journal of Physical Oceanography*, *37*(4), 982–1000, doi:10.1175/JPO3097.1.

Redi, M. H. (1982), Oceanic Isopycnal Mixing by Coordinate Rotation, *Journal of Physical Oceanography*, *12*, 1154–1158.

Sainz-Trápaga, S., and T. Sugimoto (2000), Three-dimensional velocity field and cross-frontal water exchange in the Kuroshio Extension, *Journal of Oceanography*, *56*, 79–92.

Samelson, R. M. (1992), Fluid Exchange across a Meandering Jet, doi:10.1175/1520-0485(1992)022⟨0431:FEAAMJ⟩2.0.CO;2.

Sasaki, Y. N., and S. Minobe (2015), Climatological mean features and interannual to decadal variability of ring formations in the Kuroshio Extension region, *Journal of Oceanography*, *71*, 499–509.

Sedwick, P. N., T. M. Church, A. R. Bowie, C. M. S. Marsay, J. Ussher, K. M. Achilles, P. J. Lethaby, R. J. Johnson, M. M. Sarin, and D. J. McGillicuddy (2005), Iron in the Sargasso Sea (Bermuda Atlantic Time-series Study region) during summer: Eolian imprint, spatiotemporal variability, and ecological implications, *Global Biogeochemical Cycles*, *19*, GB4006, doi:10.1029/2004GB002445.

Simmons, H. L., S. R. Jayne, L. C. St. Laurent, and A. J. Weaver (2004), Tidally driven mixing in a numerical model of the ocean general circulation, *Ocean Modelling*, *6*, 245–263, doi:10.1016/S1463-5003(03)00011-8.

Smith, S. K., and J. Marshall (2009), Evidence for Enhanced Eddy Mixing at Mid-depth in the Southern Ocean, *Journal of Physical Oceanography*, *39*, 50–69, doi:10.1175/2008JPO3880.1.

Solomon, H. (1971), On the Representation of Isentropic Mxing in Ocean Circulation Models, *Journal of Physical Oceanography*, *1*, 233–234.

Spall, M. A. (1992), Cooling Spirals and Recirculation in the Subtropical Gyre, *Journal of Physical Oceanography*, *22*(5), 564–571, doi:10.1175/1520-0485(1992)022⟨0564:CSARIT⟩2.0.CO;2.

Stommel, H. M. (1958), *The Gulf Stream: A physical and dynamical description*, 234 pp., Berkeley: University of California Press.

Takahashi, T., S. C. Sutherland, R. Wanninkhof, C. Sweeney, R. A. Feely, D. W. Chipman, B. Hales, G. Friederich, F. Chavez, C. Sabine, A. Watson, D. C. E. Bakker, U. Schuster, N. Metzl, H. Yoshikawa-Inoue, T. Steinhoff, M. Ishii, T. Midorikawa, Y. Nojiri, A. Ko, M. Hoppema, J. Olafsson, T. S. Arnarson, B. Tilbrook, T. Johannessen, A. Olsen, R. Bellerby, C. S. Wong, B. Delille, N. R. Bates, and H. J. W. de Baar (2009), Climatological mean and decadal change in surface ocean pCO2 , and net sea-air CO2 flux over the global oceans, *Deep Sea Research Part II: Topical Studies in Oceanography*, *56*, 554–577, doi:10.1016/j.dsr2.2008.12.009.

Teng, Y.-C., F. W. Primeau, J. K. Moore, M. W. Lomas, and A. C. Martiny (2014), Global-scale variations of the ratios of carbon to phosphorus in exported marine organic matter, *Nature Geoscience*, *7*, 895–898.

Trenberth, K. E., and J. M. Caron (2001), Estimates of meridional atmosphere and ocean heat transports, *Journal of Climate*, *14*, 3433–3443.

Williams, R. G., and M. J. Follows (1998), The Ekman transfer of nutrients and maintenance of new production over the North Atlantic, *Deep Sea Research Part I: Oceanographic Research Papers*, *45*, 461–489.

Williams, R. G., and M. J. Follows (2003), Physical Transport of Nutrients and the Maintenance of Biological Production, in *Physical Transport of Nutrients and the Maintenance of Biological Production*, edited by M. J. Fasham, chap. 2, pp. 19–51, Springer, doi:10.1007/978-3-642-55844-3.

Williams, R. G., V. Roussenov, and M. J. Follows (2006), Nutrient streams and their induction into the mixed layer, *Global Biogeochemical Cycles*, *20*, GB1016, doi:10.1029/2005GB002586.

Wilson, C., and V. J. Coles (2005), Global climatological relationships between satellite biological and physical observations and upper ocean properties, *Journal of Geophysical Research*, *110*, C10,001, doi:10.1029/2004JC002724.

Worthington, L. V. (1959), The 18° water in the Sargasso Sea, *Deep-Sea Research*, *2*, 297–305.

Wu, J., W. Sunda, E. A. Boyle, and D. M. Karl (2000), Phosphate depletion in the western north atlantic ocean, *Science*, *289*(5480), 759–762, doi:10.1126/science.289.5480.759.

Zhang, Z., W. Wang, and B. Qiu (2014), Oceanic mass transport by mesoscale eddies, *Science*, *345*, 322–324.

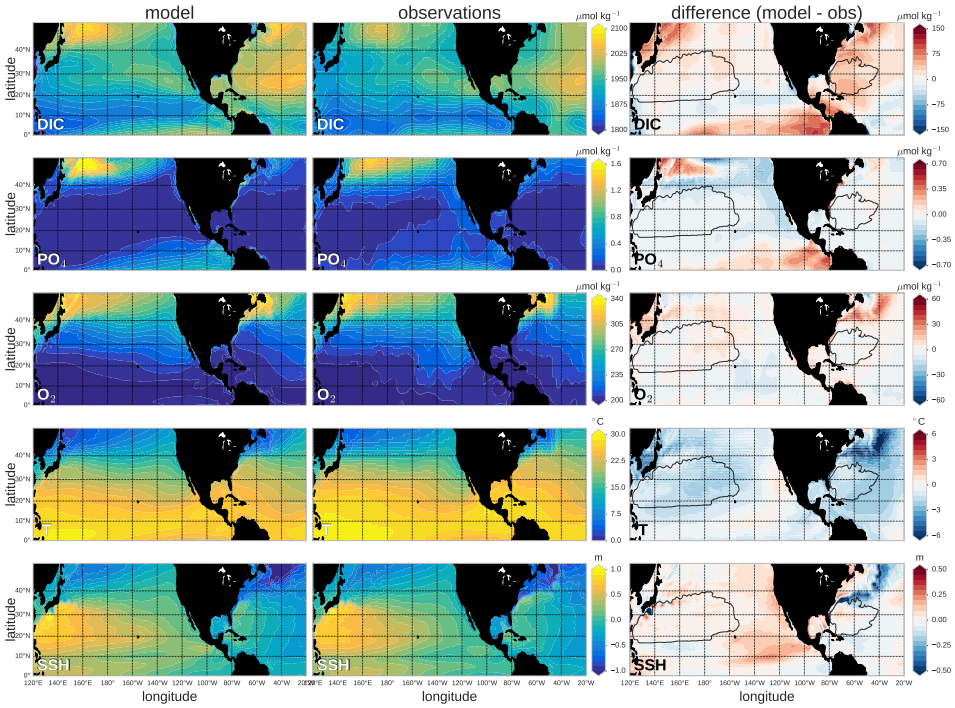

Figure 1. Surface fields for (left) the average over the last 10 years of the CM2.6-miniBLING preindustrial control simulation, (centre) observations, and (right) the difference between the CM2.6-miniBLING simulation and observations (modelled field - observation), for (top to bottom) DIC (μmol kg^{-1}), PO_4 (μmol kg^{-1}), O_2 (μmol kg^{-1}), temperature (°C), and sea surface height (SSH; m). The modelled PO_4 field is compared with the observed $PO_4/2 + NO_3/32$, as described in Section 2.1 in the text and labelled "PO_4". The observational fields of temperature, PO_4, NO_3 and O_2 are from the World Ocean Atlas 2009 [*Locarnini et al.*, 2010; *Garcia et al.*, 2010a, b], DIC from GLODAP corrected to preindustrial values [*Key et al.*, 2004] and SSH from the satellite-based analysis of AVISO from 1993 to 2010 [*Ducet et al.*, 2000]. The observational fields are interpolated onto the CM2.6 grid cells. The global mean SSH value is subtracted from both the observed and the modelled SSH datasets in order to make them comparable. The black contours shown on the right panel indicate the location of the 10-year mean subtropical gyre boundary in both basins (see Figure 2 for the gyre boundary positions of all months and Section 2.2.1 for a definition of the gyre horizontal boundaries).

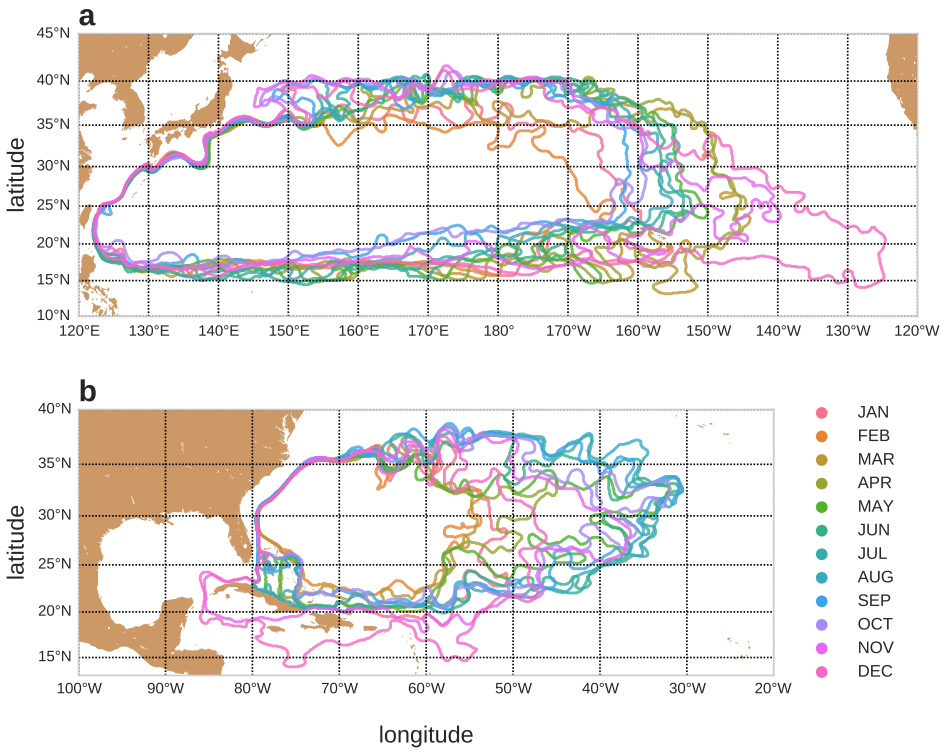

Figure 2. Monthly climatological positions of the subtropical gyres in this study, defined by using monthly mean two-dimensional barotropic mass quasi-stream function integrated over the upper 1,000 m. a) $\Psi = 20$ Sv was chosen for the North Pacific and b) $\Psi = 25$ Sv was chosen for the North Atlantic subtropical gyres as the quasi-stream function that encloses the largest areal extent over the whole year.

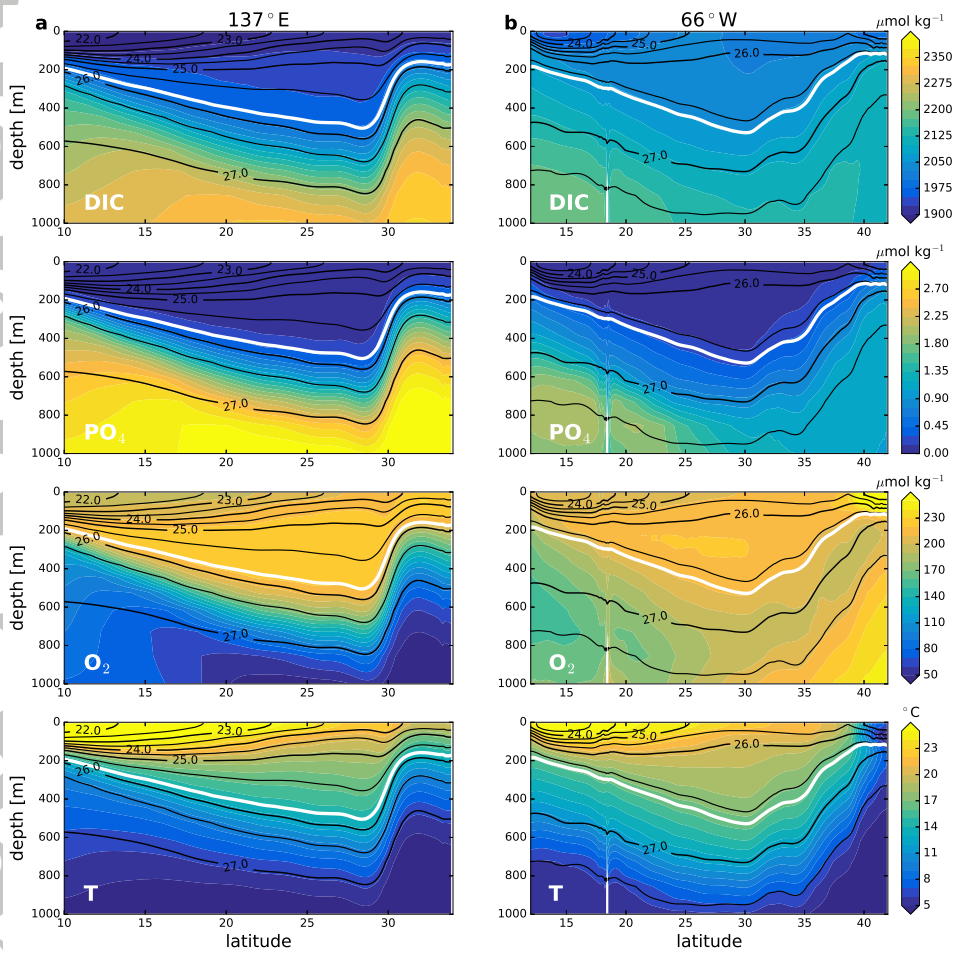

Figure 3. Ten-year mean modelled properties along a) 137 °E in the North Pacific and b) 66 °W in the North Atlantic. (Top to bottom) DIC (μmol kg^{-1}), PO_4 (μmol kg^{-1}), O_2 (μmol kg^{-1}), and temperature (°C) plotted in colour, with potential density overlaid with black contours. The isopycnal chosen for the vertical extent of the subtropical gyre for each basin in this study (σ_θ = 25.8 kg m^{-3} in the North Pacific, and σ_θ = 26.6 kg m^{-3} in the North Atlantic) is highlighted with a thick white contour on each panel.

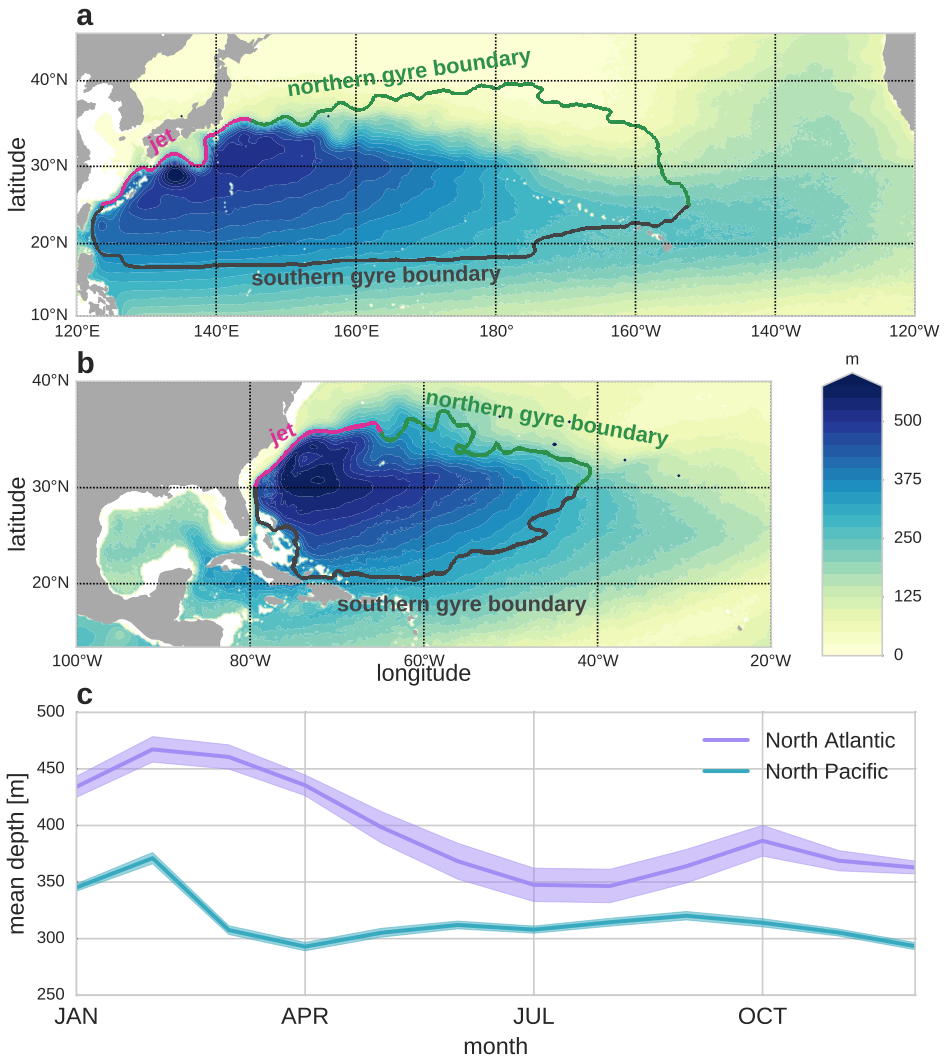

Figure 4. Annual-mean depth of the ventilated pycnocline for a) the North Pacific and b) the North Atlantic basins (colour shades). We divide the gyre boundary (coloured thick lines in panels a and b) into three segments: magenta for the jet region (i.e. the Kuroshio and Gulf Stream), green for the northern gyre boundary (north of 25°N for North Pacific and 30°N for North Atlantic), and black for the southern gyre boundary. These lines are drawn using the 10-year mean barotropic mass quasi-stream function, as described in Section 2.2.1. c) Monthly variability of the area-weighted mean ventilated pycnocline depth for (cyan) the North Pacific and (purple) the North Atlantic subtropical gyres (thick lines) and one standard deviation of the interannual variability (shaded envelopes).

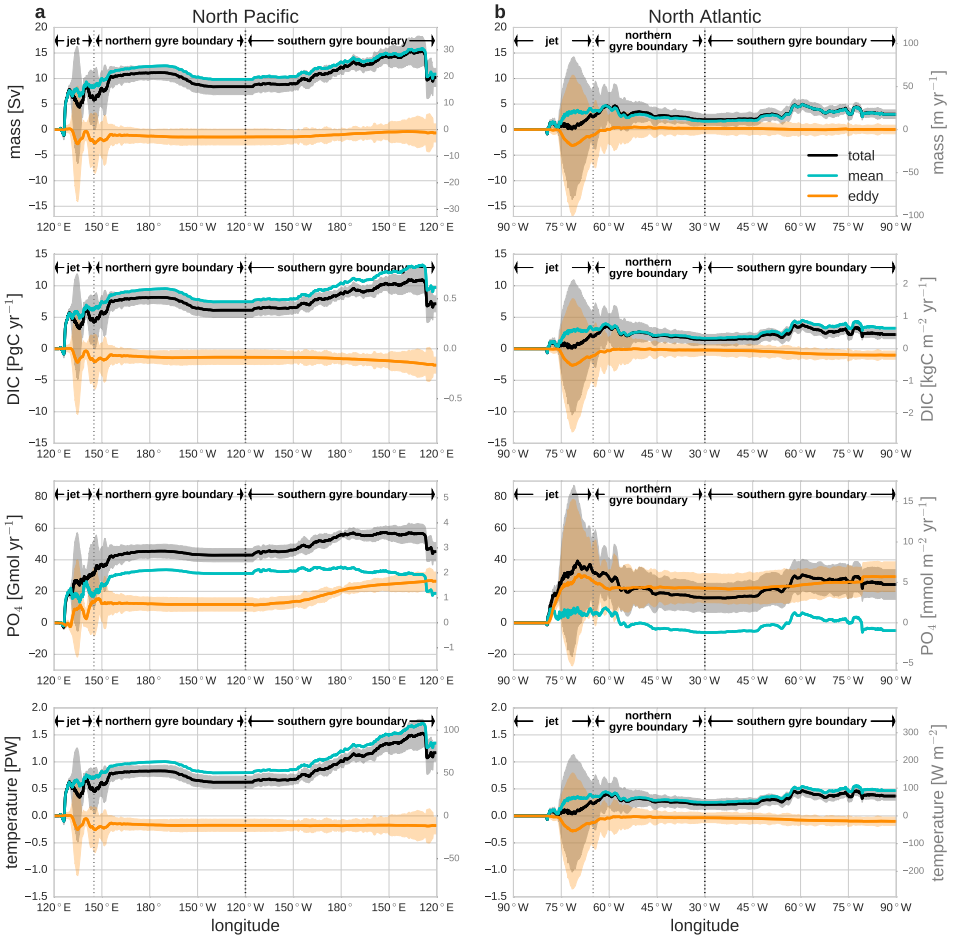

Figure 5. The cumulative sum of the 10-year average horizontal transport across the subtropical gyre boundaries, integrated vertically to the base of the ventilated pycnocline (Section 2.2.2) for a) the North Pacific and b) the North Atlantic. The total transport is shown in black, the mean transport in cyan, and the eddy transport in orange. The envelopes around the total and eddy components indicate one standard deviation of their interannual variability. The cumulative sum is taken along the boundary in the clockwise direction, starting from the westernmost edge of the jet region and plotted as a function of longitude (see Figure 4a and b for the mean position of the jet and the northern and southern gyre boundaries). The annual mean is constructed by weighting the monthly transport by the fraction of the year that the quasi-stream function is located at each longitude (Figure 2). The right-hand y-axis gives the cumulative sum of the cross-boundary transport divided by the annual-mean gyre area. For the mass transport, additional division by a reference seawater potential density of $\rho_0 = 1035$ kg m^{-3} converts mass Sv (10^9 kg s^{-1}) to a velocity with a unit of m s^{-1}. Temperature transport (Sv °C) is expressed as equivalent heat transport in PW after multiplying by heat capacity. The sign convention is such that an increase in the cumulative sum indicates inward transport into the subtropical gyre.

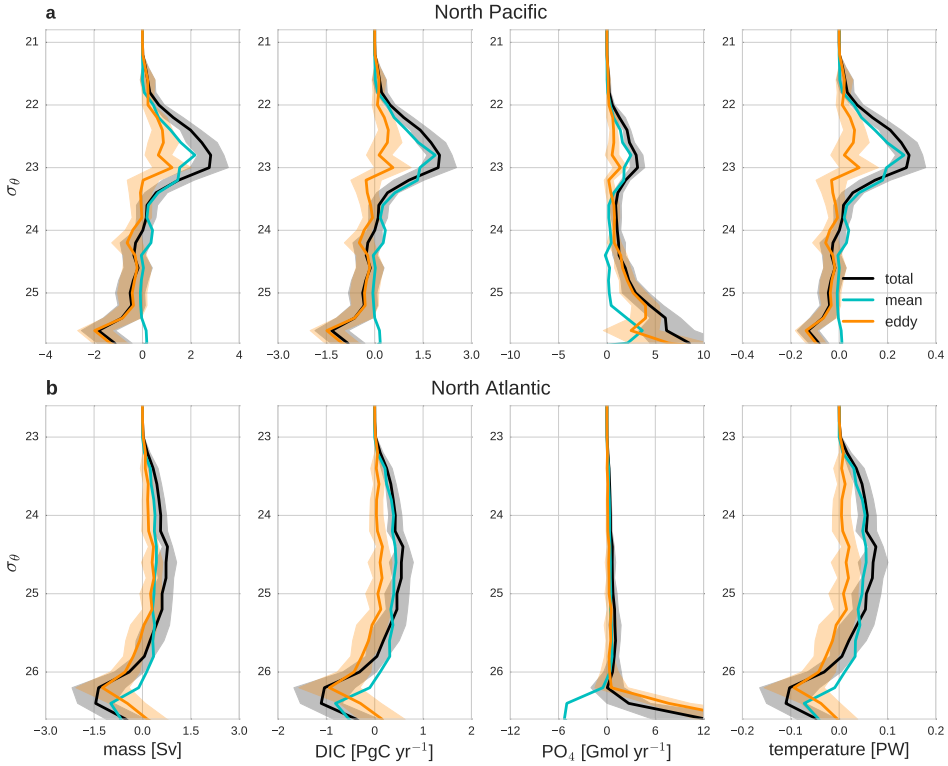

Figure 6. The 10-year averaged tracer transport across the subtropical gyre boundaries for total (black), mean (cyan), and eddy (orange) components for a) the North Pacific and b) the North Atlantic, binned into isopycnal layers. The deepest density level shown corresponds to the isopycnal at the base of the ventilated pycnocline, as defined in Section 2.2.2. The envelopes around the total and eddy components indicate one standard deviation of their interannual variability. The sign convention is such that positive values indicate transport into the subtropical gyre. Temperature transport (Sv °C) is expressed as equivalent heat transport in PW.

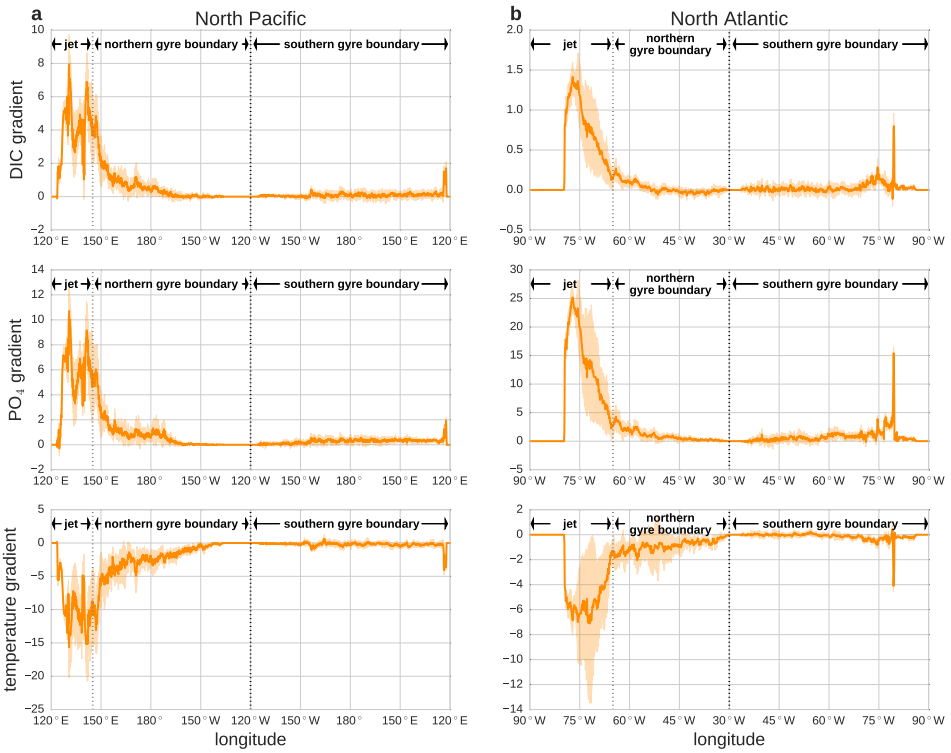

Figure 7. Cross-boundary tracer gradients. Gradients are computed along the subtropical gyre boundary for a) the North Pacific and b) the North Atlantic basin, averaged over the ventilated pycnocline, and plotted as a function of longitude in a clockwise manner starting from the westernmost edge of the jet region (see Figure 4a and b for the mean boundary locations). The tracer gradient for each month is averaged at each longitude and the annual mean is constructed by weighting the monthly-mean gradients by the fraction of the year that the quasi-stream function is located at each longitude. We choose a sign convention such that a positive gradient means the tracer has lower value inside the subtropical gyre compared to outside. With this convention, down-gradient mixing would correspond with a positive tracer input into the gyres. The thick line indicates the annual mean, while the shading indicates one standard deviation of its interannual variability. The tracer gradients are normalized by the average, large-scale, basin-wide gradient (tracer concentration difference between inside the subtropical gyre and outside, divided by the entire length scale from the centre of the subtropics to the exterior) within [10 °N - 45 °N]× [120 °E -120 °W] for North Pacific and [10 °N - 45 °N]× [90 °W - 30°W] for North Atlantic over the top 500 m depth.

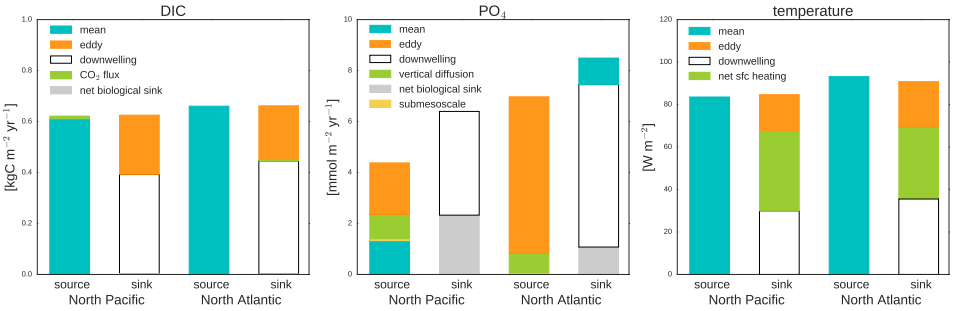

Figure 8. Annual-mean DIC (left), PO_4 (middle) and temperature (right) budgets for the North Pacific and North Atlantic subtropical gyres. "Mean" (cyan) corresponds to the mean horizontal advective transport of each tracer, "eddy" (orange) the eddy horizontal advective transport, and "downwelling" (white) the transport across the isopycnal at the base of the ventilated pycnocline, computed as the residual between the 3D advective convergence within the gyre bowl and the total cross-boundary horizontal transport. "CO_2 flux" (green on the left panel) is the air-sea CO_2 flux; "net biological sink" (grey on the left panel) is the biological consumption and remineralization of DIC; "vertical diffusion" (green on the middle panel) is the flux of PO_4 across the bottom of the layer via parameterized vertical mixing; "net biological sink" (grey on the middle panel) corresponds to the net biological consumption of PO_4 integrated over the vertical layer; "submesoscale" (yellow on the middle panel) is the PO_4 supply due to the parameterization of submesoscale mixed layer instabilities; and "net sfc heating" (green on the right panel) is the net surface heating including the effect of longwave and shortwave penetrating radiation, as well as sensible and latent heat fluxes. Additional terms, including vertical diffusion and submesoscale transport of DIC and temperature are all at least three orders of magnitude smaller than the shown terms, and therefore excluded from the figure. Note that the imbalance between the source and sink particularly evident for PO_4 is due to the non-negligible tendency term, amounting to -2.3 mmol m^{-2} yr^{-1} for the North Pacific and -1.5 mmol m^{-2} yr^{-1} for the North Atlantic subtropical PO_4 budgets. This imbalance is associated with a time tendency in the model over the 10-year period we analyzed.

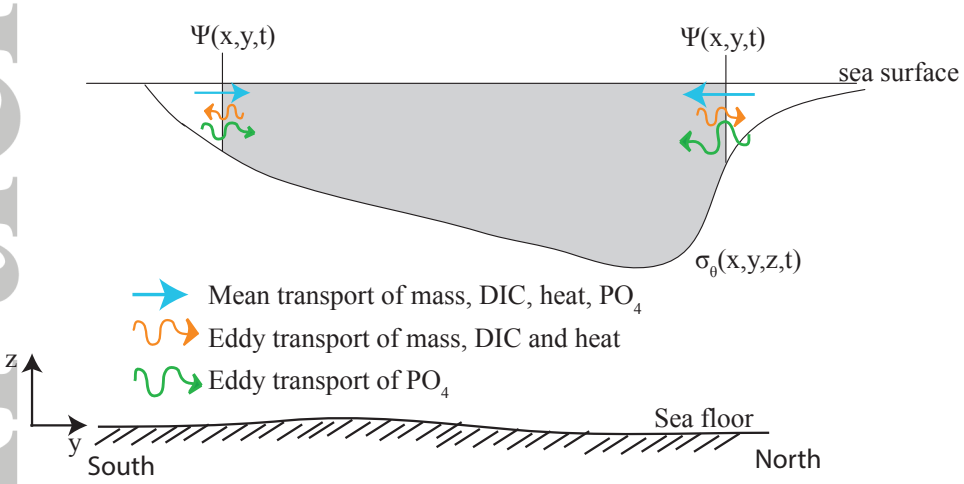

Figure 9. Schematic of mass and tracer horizontal, cross-boundary transport on a cross-section of the subtropical gyres. The horizontal boundary, defined in Section 2.2.1, is denoted by the vertical straight lines labelled $\Psi(x, y, t)$. The curved line labelled as $\sigma_\theta(x, y, z, t)$ shows the time-varying vertical limit of the subtropical gyre (the grey shaded area), defined in Section 2.2.2. The asymmetry in the depth of the gyre bowl represents the meridional contrast in the depth of the ventilated pycnocline as can be seen in Figure 4. The straight arrows in cyan indicate the mass and tracer time-mean advective cross-boundary transport. Wavy arrows show the eddy cross-boundary transport for mass, DIC and heat (orange) and PO_4 (green). For simplicity, we do not include the small outward time-mean PO_4 flux in the North Atlantic, which arises from a small outward advection at the base of the chosen layer that is multiplied by the heightened PO_4 concentrations on the layer as noted in Section 3.2.